Evaluating the performance of WRF urban schemes and PBL schemes over Dallas Fort Worth during a dry summer and a wet summer

Jinxin Wang[1,2], Xiao-Ming Hu[1]

[1]Center for Analysis and Prediction of Storms, and School of Meteorology, University of Oklahoma, Norman Oklahoma 73072

[2]National Supercomputing Center in Wuxi, Wuxi, 214011, China

Corresponding author address:

Jinxin Wang

Center for Analysis and Prediction of Storms

The University of Oklahoma,

120 David L. Boren Blvd, Norman OK 73072

jwang@ou.edu

Abstract

This study evaluated the Weather Research and Forecasting (WRF) model sensitivity to different planetary boundary layer (PBL) schemes (the YSU and MYJ schemes) and urban schemes including the bulk scheme (BULK), single-layer urban canopy model (UCM), multi-layer building environment parameterization (BEP) model, and multi-layer building energy model (BEM). Daily reinitialization simulations were conducted over Dallas-Fort Worth during a dry summer month (July 2011) and a wet summer month (July 2015) with weaker (stronger) daytime (nocturnal) UHI in 2011 than 2015. All urban schemes overestimated the urban daytime 2m temperature in both summers, but BEP and BEM still reproduced the daytime urban cool island in dry summer. All urban schemes reproduced the nocturnal urban heat island, with BEP producing the weakest one due to its unrealistic urban cooling. BULK and UCM overestimated the urban canopy wind speed, while BEP and BEM underestimated it. The urban schemes showed prominent impact on daytime PBL profiles. UCM+MYJ showed a superior performance than other configurations. The relatively large (small) aspect ratio between building height and road width in UCM (BEM) was responsible for the overprediction (underprediction) of urban canopy temperature. The relatively low (high) building height in UCM (BEM) was responsible for the overprediction (underprediction) of urban canopy wind speed. Improving urban schemes and providing realistic urban parameters were critical for improving urban canopy simulation.

1. Introduction

Cities are facing increasing challenges with growing global urbanization (Georgescu et al. 2014). Nowadays, more than half of the world's population live in cities, and this percentage is expected to reach two thirds in the following half-century (United Nations Department of Economic and Social Affairs 2012). Urbanization alters the local weather and climate (e.g., urban heat island (UHI)) and threatens the comfort of the residents. Due to lack of dense surface and upper-level observation, numerical models are often utilized to better understand the urban impact on local weather and climate.

There are four urban schemes coupled with the Weather Research and Forecasting (WRF) model. The first urban scheme is a bulk (BULK) scheme. It increases heat capacity and thermal conductivity to represent urban heat storage and enhances roughness to represent sink of momentum and generation of turbulence (Taha 1999; Liu et al. 2006). Its disadvantage is that it cannot represent the heterogeneity of urban variability among different neighborhoods (Salamanca et al. 2011). Reames and Stensrud (2017) separated single urban class into three urban classes to improve BULK's performance. Since WRF version 3.7, detailed urban classification was implemented for BULK through incorporating the National Land Cover Database (NLCD) into the WRF Pre-Processing System (WPS).

The second urban scheme is the single-layer Urban Canopy Model (UCM) (Kusaka et al. 2001; Kusaka and Kimura 2004a, 2004b). It consists of two-dimensional symmetrical street canyons with infinite length and three urban surfaces (Kusaka et al. 2001). Though the geometry of the city is simplified, the radiation treatment in urban canopy is three-dimensional (Kusaka et al. 2001). UCM uses three different urban classes with different

thermal and roughness properties to represent urban heterogeneity. UCM uses approximately 30 input parameters for the thermal properties. Among these parameters, urban fraction plays a dominant role in modulating latent heat flux (Nemunaitis-Berry et al. 2017), because urban fraction determines the relative contribution of urbanized and vegetated landscapes to the total flux.

The third urban scheme is the multi-layer Building Environment Parameterization (BEP) model. BEP introduces a scheme to represent the impact of urban buildings on resolved airflow (Martilli et al. 2002). BEP can reproduce the increase of Reynolds stress profiles with height, store more energy in the urban fabric during the day, and reduce the turbulence intensity below the average roof height by changing the length scale (Martilli 2002; Martilli et al. 2002).

The fourth urban scheme is multi-layer Building Energy Model (BEM). BEM is added to BEP to reproduce the generation of heat in buildings and the way heat is exchanged with the exterior flow (Salamanca et al. 2009). BEM considers heat diffusion through walls, roofs, and floors; natural ventilation; the radiation exchange between indoor surfaces; the generation of heat due to occupants and equipment; and the consumption of energy due to air conditioning (AC) systems (Salamanca et al. 2009). An offline evaluation of BEM against BEP showed that BEM satisfactorily produced the urban fluxes (Salamanca and Martilli 2009). Consequently, BEM might lead to a better simulation of UHI and urban boundary layer (Salamanca and Martilli 2009).

Efforts have been paid to evaluate the four schemes' performance within the WRF model. BULK and UCM can be coupled with any planetary boundary layer (PBL) schemes in WRF, while BEP and BEM are currently coupled only with two local PBL schemes, the

92 Mellor–Yamada–Janjić (MYJ) (Janjić 1990; Janjic 1994) and the Bougeault–Lacarrére
93 (BouLac) (Bougeault and Lacarrere 1989). Hendricks et al. (2020) achieved positive
94 outcomes when coupling BEP/BEM with modified YSU scheme in their experiments.
95 Salamanca et al. (2011) found that all urban schemes except BULK underestimate the air
96 temperature, and UCM overestimated the wind speed while BEP and BEM underestimated
97 it. Liao et al. (2014) concluded that BULK scheme was suitable for real-time weather
98 forecast and multi-layer urban scheme was beneficial for studying the impact of
99 urbanization on regional climate. Gutierrez et al. (2015) found that BULK tended to
100 overestimate daytime wind speed and daytime temperature. Jänicke et al. (2017) concluded
101 that BULK performed better than the UCM and BEP, and the BouLac performed better
102 than MYJ. Sharma et al. (2017) found BEM with High-Resolution Land Data Assimilation
103 System (HRLDAS) had quite low model bias and root mean square error for both during
104 day and night.

105 Albeit these previous evaluations, the performance of urban and PBL schemes and
106 its influence factors remain inconclusive. Observational climatology studies appeared to
107 suggest that the UHI intensity had a close relation with humidity, with strong UHI in dry
108 scenarios and weak UHI in wet scenarios (Winguth and Kelp 2013; Hu et al. 2016).
109 However, the background mechanism remains elusive. In this study, we aimed to evaluate
110 the urban and PBL schemes' performance in different humidity scenarios and attempted to
111 explain the reason for their performance. To this end, we conducted daily simulation over
112 a dry summer month (July 2011) and a wet summer month (July 2015). In addition to
113 examining model sensitivity to different PBL and urban schemes, different characteristics
114 of urban effects and their causative factors during the two months were also investigated.

115 In the following, Section 2 describes selected episodes, observational datasets, and
116 model configurations; Section 3 evaluates model performance against surface observation
117 and sounding, particularly in terms of model capability to simulate urban effects including
118 both thermal and dynamic effects; Section 4 gives the conclusion.

119 ## 2. Model setup and Data

120 2.1. Model configuration

121 The WRF model (version 3.8) was employed to conduct the simulation over the
122 two months. Four two-way nested domains were at 27km (D1, 190×160), 9km (D2,
123 190×160), 3km (D3, 190×160), 1km (D4, 205×235) spatial resolution (Figure 1a), with 48
124 levels extending from the surface to 100hPa. The heights of the lowest 27 levels are listed
125 in Table 3. The innermost domain, D4, covers both the DFW urban region and its
126 surrounding rural region. All the following model analysis was based on the simulation
127 result of D4. The initial and boundary conditions were from North American Regional
128 Reanalysis (NARR) dataset. All experiments were initialized at 12:00 UTC (06:00 CST)
129 every day from June 30th to July 30th and simulated for 47 hours. The boundary conditions
130 were updated every 3 hours. The first 23 hours were discarded as model spin-up, the
131 remaining 24 hours were used for analysis. The physics schemes used for this study
132 included WRF single-moment six-class (WSM6) microphysics scheme (Hong et al. 2004),
133 the Rapid Radiative Transfer Model longwave radiation scheme (Mlawer et al. 1997), the
134 Dudhia shortwave radiation scheme (Dudhia 1989), the Eta surface layer scheme (Janjic
135 1994), the MYJ PBL scheme (Janjic 1994), the Noah Land Surface Model (Chen and
136 Dudhia 2001), and the four urban schemes. The Kain-Fritsch cumulus scheme (Kain 2004),
137 was applied for the D1 and D2. One additional set of simulation with UCM coupled with

YSU PBL scheme (Hong et al. 2006) was conducted, comparing with UCM+MYJ to evaluate the PBL schemes' impact on urban atmosphere simulation. In simulation of real cases, BEM usually worked with BEP, which was named as BEP+BEM in previous studies, but in this study we named it as BEM for simplicity.

2.2. Land-use category update

The heterogeneity of land-use category is one of the reasons for the heterogeneity of near-surface meteorological variables. Therefore, an up-to-date high-resolution land cover dataset becomes important for reliable simulation of the urban atmosphere. The original 24-class USGS land cover data with its finest spatial resolution 30 seconds (~1km) was collected in the early 1990s, and much of the land cover has measurably changed after two decades. The 20-class NLCD 2011 with 30m spatial resolution is an up-to-date high-resolution land cover database over U. S. By integrating the 20-class NLCD 2011 and the 20-class MODIS (Wickham et al. 2015), the US Environmental Protection Agency produces the 40-class NLCD 2011 (see the NLCD over the DFW region in Figure 1b). The percentage of the three urban classes (high, medium, low intensity) were also derived from NLCD 2011, which are 0.1, 0.16, 0.74 over DFW.

The National Urban Database and Access Portal Tool (NUDAPT) provides additional information with a resolution of 1 km^2 for urban parameterization (Ching et al. 2009). The NUDAPT contains the urban morphology of 44 cities in the United States.

2.3. Anthropogenic heat update for UCM

There are two major energy sources over the urban land surface: net radiation and anthropogenic heat (AH). In UCM, the diurnal AH profile has a close relation with urban

density. The default values of maximum hourly AH in WRF are $90\mathrm{Wm}^{-2}$, $50\mathrm{Wm}^{-2}$, $20\mathrm{Wm}^{-2}$ respectively for the commercial, high-intensity residential, and low-intensity residential urban land-use categories. Different cities have different AH profiles. Efforts for creating proper AH profiles for major cities have been made in recent years. Based on US National Emission Inventory year 2005 data, Lee et al. (2014) reported that the summertime maximum AH over 4km × 4km grid cells of DFW was $65.9\mathrm{Wm}^{-2}$ and the city-scale averaged maximum AH of DFW was $17.4\mathrm{Wm}^{-2}$. With consideration of multiple datasets, including electricity data and transportation data, Sailor et al. (2015) reported that the summertime city-scale averaged maximum summer AH in DFW was $13.99\mathrm{Wm}^{-2}$, and provided an updated hourly AH profile. In this study, based on Sailor et al. (2015), a simple approach was designed to derive the diurnal maximum AH, with the ratio of maximum AH of high, medium, low intensity urban area assumed to be 9:5:2 and city-wide averaged AH to be 13.99 Wm^{-2}. With these assumptions, one could derive that the diurnal maximum AH for the three urban types are $39.4\mathrm{Wm}^{-2}$, $21.9\mathrm{Wm}^{-2}$, $8.8\mathrm{Wm}^{-2}$, respectively. The updated AH profiles for the three urban classes were shown in Figure 1c. The default AH parameters in BEP and BEM were also recommended to be updated (Salamanca et al. 2011; Liao et al. 2014; Gutierrez et al. 2015; Salamanca et al. 2015; Sharma et al. 2017). However, because of the lack of official document about the DFW urban parameters for BEP and BEM, the parameters in BEP and BEM kept as default in this study.

2.4. Sensitivity study of urban geometry parameters

Previous studies have confirmed that urban geometry had significant effect on urban energy budget (Oke 1982; Stewart and Oke 2012). The urban geometry can be described by a few variables including sky view factor (SVF) and aspect ratio (AR)

(Stewart and Oke 2012), which can be further derived from building height (BH), road width (RDW), and roof width (RFW).

The urban geometry parameters in UCM and BEM adopted in the control experiments (UCM-CTRL and BEM-CTRL) were listed in Table 4 and Table 5, respectively. The default BH in UCM-CTRL was lower than that in BEM-CTRL, which was suspected as the reason for the larger canopy wind speed in UCM-CTRL than that in BEM-CTRL. For studying the impact of BH on canopy wind speed, UCM-HBH adopted higher building height (HBH) and BEM-LBH adopted lower building height (LBH). The BH in BEM-LBH was same as the BH in UCM-CTRL, while the BH in UCM-HBH was lower than the BH in BEM-CTRL because UCM was not allowed to adopt a BH higher than the first model level. For studying the impact of RDW and RFW on urban canopy atmosphere, BEM-LBH-NRDW based on BEM-LBH adopted narrower RDW (same to the RDW in UCM-CTRL) and BEM-LBH-NRDW-NRFW based on BEM-LBH-NRDW adopted narrower RFW (same to the RFW in UCM-CTRL). Therefore, the urban geometry parameters in BEM-LBH-NRDW-NRFW were same as those in UCM-CTRL. All experiments in this part were initialized at 12:00 UTC (06:00 CST) June 30th, 2011, and ended at 11:00 UTC (05:00 CST) July 1st, 2011. The boundary conditions were updated every 3 hours. The first 23 hours were discarded as model spin-up, the remaining 24 hours were used for analysis. All other physics schemes remained same.

2.5. Observation data

Texas Commission on Environmental Quality (TCEQ) observation network was used to evaluate simulated near surface variables. TCEQ data were proven reliable for UHI analysis (Winguth and Kelp 2013; Hu and Xue 2016). There were 26/40 stations available

during July 2011/2015, respectively (see Fig. 2 for their locations). According to the NLCD land-use category, 8 (16) urban stations were within DFW urban area during July 2011 (2015) (Figure 2a, b). However, the land-use category is not the only reference to identify the station type. Thermal inertia is another key factor to distinguish urban sites from rural sites. During the early evening transition period, the urban cooling rates were lower than the rural cooling rates, and the cooling rates difference between the two summers was also noticeable (Figure 2c, d). The cooling rates during the wet summer were lower than the cooling rates during the dry summer (Figure 2c, d), which meant the near-surface atmosphere had larger thermal inertia during the wet summer than during the dry summer, because of the soil moisture difference between the two summers. With consideration of both land-use category and thermal inertia, 5 TCEQ urban stations were chosen for model verification. All the 5 stations had a record of 2m temperature and 10m wind speed, but only 2 stations, Dallas Hinton and Fort Worth Northwest, have records of temperature of dewpoint (TD).

The 1-second resolution SPARC (Stratosphere-troposphere Process And their Role in Climate) sounding at Fort-Worth upper air station (97.29806°W, 32.83500°N) (blue star in Figure 2) during July 2011 and July 2015 was used for verifying simulated profiles. The SPARC soundings were launched twice each day, one from 0500 CST to 0700 CST and another from 1700 CST to 1900 CST.

3. Results

3.1. Diurnal variation of urban canopy temperature, wind speed, RH, and TD

All urban schemes over predicted the daytime 2m temperature in both summers (Figure 4a, b). Among the four urban schemes, BULK gave the largest over-prediction of 2m temperature at both daytime and nighttime in the two summers (Figure 4a, b). In dry summer, UCM gave the second-largest over-prediction of daytime 2m temperature (Figure 4a), while in wet summer, UCM simulated similar daytime 2m temperature to BEP and BEM. In both summers, the performance of BEP was almost same to that of BEM at daytime, but BEP cooled the city much faster at nighttime (Figure 4a, b). This was because the indoor temperature of BEP was fixed to 298K (25℃) which was lower than the outdoor temperature in summer. As a result, the building became a thermal sink and produced toward building heat flux at night. We can imagine that BEP would overpredict urban air temperature when the indoor temperature would be higher than the outdoor temperature. UCM+YSU produced higher nocturnal near-surface temperature than UCM+MYJ (Figure 4a, b), because of stronger PBL vertical mixing by YSU, which transported the warmer upper air down to the surface.

BULK and UCM predicted stronger wind speed than observation, while BEP and BEM predicted more realistic wind speed (Figure 4c, d). This is because BULK and UCM use a roughness length that is not directly dependent on urban morphology, while BEP and BEM estimate the momentum sink with a drag force that depends on urban morphology (Salamanca et al. 2011). By adjusting the roughness length for the urban category, Reames and Stensrud (2017) improved BULK's performance on simulating urban wind speed. Hu et al. (2016) contributed the overestimation of urban wind speed in UCM to the overestimation of vertical transport of momentum. BULK+MYJ produced larger nocturnal near-surface urban wind speed than UCM+MYJ (Figure 4c,d). UCM+YSU produced

larger nocturnal near-surface wind speed than UCM+MYJ (Figure 4c, d), because of stronger vertical mixing by YSU. The wind speed simulation contrast between urban schemes and PBL schemes suggested that the vertical transport of momentum does take effect on urban wind simulation. However, improving urban schemes would bring more significant effect on urban wind simulation. Barlage et al. (2016) pointed out the dynamic reason why BEP and BEM performed better than BULK and UCM in urban canopy wind simulation: BULK and UCM were separated from the atmosphere above and communicated with the above atmosphere only with bulk surface flux and grid-scale roughness length, while BEP and BEM allowed buildings to protrude into the lower atmosphere and were more direct and realistic in capturing building drag effect.

Because of the significant negative relationship between RH and temperature, the performance of the four urban schemes on RH prediction was reversed to that on temperature prediction. All urban schemes tend to underpredict the daytime RH, especially in wet summer (Figure 4e, f). As TD is less sensitive to temperature, the simulation of TD was evaluated to better understand the urban schemes' performance on urban humidity prediction. In both summers, all models tend to overpredict the TD at daytime and underpredict the TD at nighttime (Figure 4g, h). In dry summer, UCM+YSU predicted the lowest daytime TD. In wet summer, BULK+ MYJ predicted the lowest daytime TD, while UCM+MYJ predicted the highest daytime TD (Figure 4g, h). The TD predicted by BEP and BEM were almost the same (Figure 4g, h). The TD diurnal profiles by all models deviated much more away from observation in wet summer than in dry summer, because the low-resolution WRF initialization data from NARR could not resolve the heterogeneity of soil moisture in wet summer. In dry summer, the simulated TD diurnal profiles were

closer to observation, because it was too dry within the city and the urban soil moisture heterogeneity was reduced. Some studies used the High-Resolution Land Data Assimilation System (HRLDAS) to improve the initial soil condition in WRF model (Nemunaitis-Berry et al. 2017; Reames and Stensrud 2017; Sharma et al. 2017). However, the soil moisture simulated by HRLDAS still deviated from observation, though the urban-rural contrast could be resolved (Reames and Stensrud 2017).

3.2. Diurnal variation of surface energy balance

According to Oke (1982) and Oke (1988), the surface energy balance equation is written as:

$$Q^* + Q_F = Q_H + Q_E + \Delta Q_s + \Delta Q_A \quad (1)$$

where Q^* is the net all-wave radiation, Q_F is anthropogenic energy, Q_H is sensible heat flux, Q_E is latent heat flux, ΔQ_s is stored energy, and ΔQ_A is net heat advection. The net all-wave radiation, Q^*, received by the ground is defined as:

$$Q^* = (1 - \alpha) \cdot S_{\downarrow} + \varepsilon \cdot (L_{\downarrow} - \sigma \cdot T_{skin}^4) \quad (2)$$

where α is surface albedo, ε is surface emissivity, σ is Stefan-Boltzmann constant, $S_{\downarrow}$ is downward short-wave radiation, $L_{\downarrow}$ is downward long-wave radiation, and T_{skin} is skin temperature in Kelvin.

In UCM and BEM, Q_F is added to Q_H. ΔQ_A is suggested to be negligible when the measurement is accurate (Christen and Vogt 2004). It is reported that ΔQ_s has a positive correlation with Q^* (Grimmond 1992; Christen and Vogt 2004). The positive (negative)

value of ΔQ_s means there is storing (releasing) ground heat flux. The positive (negative) value of Q^* means there is a net income (outcome) of net radiation for the surface.

The net radiation amount received by the city were similar for all urban schemes and PBL schemes in both summers (Figure 5a, b). The energy partition was more sensitive to urban schemes than to PBL schemes (Figure 5c-f). The energy partition was almost unchanged for BULK between the two summers (Figure 5c-h), because BULK treated all urban grids as concrete surface (assuming 100% urban fraction) with very high resistance to evapotranspiration (Figure 5e, f). As a result, in BULK, most energy was partitioned into sensible heat flux, which was more apparent in wet summer (Figure 5c, d). The weakest latent heat flux by BULK resulted in the lowest TD. BULK stored the most ground heat flux at daytime and released them as sensible heat flux at nighttime (Figure 5g, h), which explained why BULK predicted the highest nocturnal 2m temperature (Figure 4a, b). Reames and Stensrud (2017) modified the scaling factors that modulated evapotranspiration in response to insolation and vapor pressure deficit and achieved some improvement to BULK's performance. The weak evapotranspiration in BULK is actually caused by the underestimation of subgrid-scale variability of land surface characteristics (Li et al. 2013). Li et al. (2013) pointed out that the subgrid-scale variability of land surface characteristics continued to be important and should be accounted for, even if the resolution of numerical simulation was as high as 1 km.

UCM stored the second most ground heat flux at daytime and released the second-most ground heat flux at nighttime (green line and yellow line under green line) in Figure 5g, h, which resulted in the second-highest 2m temperature at nighttime. The latent heat flux predicted by UCM was same to that predicted by BEP and BEM (Figure 5e,f).

316 Nemunaitis-Berry et al. (2017) concluded that the urban fraction was the only UCM
317 parameter to significantly affect the latent heat flux. The urban fraction defined in the look-
318 up table in the WRF model is shared by UCM, BEP, and BEM, which is why the latent
319 heat flux is same for the three urban schemes. The sensible heat flux predicted by UCM
320 was least among these urban schemes (Figure 5c, d). The predicted net radiation, latent
321 heat flux, and ground heat flux were same between BEP and BEM, except the predicted
322 sensible heat flux. Because BEM considered the impact of AC, it produced more sensible
323 heat flux than BEP. BEP and BEM both stored the least ground heat flux at daytime and
324 released the least ground heat flux at nighttime, therefore the near-surface atmosphere
325 simulated by BEP and BEM cooled faster than that simulated by BULK and UCM.

326 3.3. Evaluation of schemes' performance at daytime

327 Daytime urban cool island (UCI) and UHI were observed in dry summer and wet
328 summer, respectively (Figure 6a, b). In dry summer, because of urban irrigation, urban soil
329 was wetter than rural soil, it was likely that urban surface released less sensible heat flux
330 than rural surface and UCI formed. On the contrary, in wet summer the surface humidity
331 was decided by stored precipitation rather than irrigation, because of urban impervious
332 surface, urban soil was drier than rural soil, and UHI formed. In observation, the urban
333 wind speed is usually weaker than the rural wind speed (Hu et al. 2016). The observed
334 daytime wind speed within the city was weaker than that in the upstream urban edge and
335 rural area, and the observed daytime wind speed in wet summer was generally stronger
336 than that in dry summer (Figure 7a, b).

337 In dry summer, all urban schemes erroneously produced daytime UHI (Figure 8a-
338 c), and the daytime UHI intensity produced by BEP and BEM was weaker than that by

BULK and UCM (Figure 8d, e). In wet summer, all urban schemes produced daytime UHI, and the simulated daytime UHI intensities from high to low were by BULK, UCM, BEM and BEP (Figure 8f-j).

At daytime, UCM+YSU could not produce the weaker urban wind speed (Figure 9c, h), while UCM+MYJ could produce weaker urban wind speed (Figure 9b, g), because the vertical momentum transport in the MYJ's local mixing was weaker than that in the YSU's nonlocal mixing, which suggested that improving PBL schemes can help improving urban wind speed simulation. However, the urban wind speed was much better simulated by BEP and BEM, which suggested that improving the urban schemes was more effective than improving the PBL schemes, because BEP and BEM estimated the momentum sink with a drag force that depended on urban morphology (Salamanca et al. 2011).

YSU predicted higher PBL height (PBLH) than MYJ (Figure 10a, b), because of stronger mixing in the nonlocal PBL scheme (Hu et al. 2010b). The Θ profiles by YSU and MYJ showed more obvious difference in wet summer than in dry summer. The shape of Θ profiles by MYJ was closer to observation than YSU. In both summers, the simulated Θ was about 2K higher than observation, because of model error and unrealistic surface properties (Hu et al. 2010a). The daytime Θ profiles were more sensitive to PBL schemes than to urban scheme. The Θ profiles in dry summer were not as sensitive as the Θ profiles in wet summer to the urban schemes.

For daytime PBL wind simulation, the PBL schemes were more dominant than the urban schemes (Figure 10c, d). YSU predicted the weakest wind speed at 400~2000m above ground, especially in wet summer. The urban schemes had obvious impacts on the daytime PBL wind profiles, because of the strong daytime coupling between surface and

362 PBL. The simulated daytime wind speed by all urban schemes was weaker than observation
363 at levels higher than 400m (200m) above ground in dry (wet) summer. The daytime PBL
364 wind speed simulated by BEP and BEM was weaker than that by BULK and UCM, because
365 BEP and BEM adopted a rougher urban surface.

366 The lapse rates and intensity of daytime QV were both not well simulated by all
367 schemes (Figure 10e, f). The errors of QV lapse rates simulation were caused by PBL
368 schemes, while the errors of QV intensity simulation were caused by the model initialized
369 soil data. In PBL schemes, all scalars, such as QV and Θ, are treated in the same way. The
370 simulation result showed that the QV profiles were not well simulated as Θ profiles, which
371 meant the QV and Θ should be treated differently in PBL schemes. The urban schemes'
372 impact on QV profiles was noticeable. BULK produced the driest PBL, because of its
373 weakest evapotranspiration. YSU predicted drier PBL than MYJ, because of its stronger
374 vertical mixing. In wet summer, BULK+MYJ and UCM+YSU showed similar
375 performance in simulating daytime QV profile in the lowest 1200m PBL (Figure 10f).
376 Both YSU and MYJ could not well simulate the sharp lapse rate of QV in the lowest 200m
377 PBL.

378 3.4. Evaluation of schemes' performance at nighttime

379 The observed nocturnal UHI in both summers did not show obvious difference in
380 their intensity (Figure 6c, d). The observed nocturnal wind speed within the city was
381 weaker than that outside the city. The observed nocturnal wind speed in wet summer was
382 not obviously stronger than that in dry summer (Figure 7c, d).

All urban schemes produced nocturnal UHI in both summers (Figure 11). The nocturnal UHI intensity was overpredicted by BULK (Figure 11a, f) and underpredicted by BEP (Figure 11d, i). The nocturnal UHI intensity produced by UCM and BEM were closer to observation (Figure 11b, c, e, g, h, j). The nocturnal UHI simulation was more sensitive to urban schemes than to PBL schemes (Figure 11).

Both BULK and UCM (no matter coupled with YSU or MYJ) predicted stronger urban wind speed than rural wind speed (Figure 12a-c, f-h), which meant properly simulating urban nocturnal wind speed remained as a challenge for PBL schemes. Previous studies have contributed the overpredicted urban wind speed to the nonproper setting of urban roughness (Reames and Stensrud 2017) and imbalance between urban schemes and PBL schemes (Hu et al. 2016).However, BEP and BEM could reasonably reproduce weaker urban wind speed (Figure 12d, e, i, j), which again proved that improving the urban schemes was more effective than improving the PBL schemes in urban wind speed simulation.

The nocturnal Θ profiles showed apparent distinction among these urban schemes (Figure 13a, b), which was caused by the different urban surface cooling rates. The patterns of nocturnal Θ profiles by YSU were closer to observation, but the intensity was about 1~2K larger than observation. BEP cooled near surface atmosphere fastest and produced the most stable nocturnal PBL. As BULK released sensible heat flux into atmosphere at nighttime, it produced the most unstable nocturnal PBL structure.

The simulated nocturnal PBL jet by MYJ had similar profiles to the observed PBL jet (Figure 13c,d), with weak impact from urban schemes, because the nocturnal surface layer was basically decoupled from PBL. YSU predicted a weaker and lower nocturnal

406 PBL jet in dry summer, while its performance was improved in wet summer. The lapse
407 rates and intensity of nocturnal QV profiles were still not well simulated (Figure 10e, f).

408 3.5. Urban geometry parameters' impact on urban temperature and wind speed

409 The default urban geometry configurations between UCM and BEM showed
410 significant distinction (Table 4 and Table 5). The default BH in BEM, almost twice as large
411 as that in UCM, was higher than the 1st model level and allowed the urban structure to
412 interact with the lower atmosphere. In UCM, BH, RDW and RFW all increased with urban
413 residential intensity. However, in BEM, BH and RFW increased with urban residential
414 intensity, while RDW decreased with urban residential intensity. In UCM (BEM), the ARs
415 between default BH and RDW were 0.6 (0.33), 0.8 (0.6) and 1.0 (1.2) for LIR, HIR and
416 IC, respectively. Considering most urban areas were LIR or HIR, the SVFs of UCM's street
417 canyons were generally smaller than that of BEM, therefore radiation energy loss in UCM
418 was less than that in BEM, which could result in higher urban temperature in UCM than in
419 BEM (Figure 14a, c).

420 In addition, in UCM (BEM), the ratios between default RFW and RDW were 1.0
421 (0.43), 1.0 (0.68) and 1.0 (1.0) for LIR, HIR and IC, respectively. Therefore, the building
422 area was more in UCM than in BEM. More radiation energy would be absorbed at daytime
423 and released at nighttime by buildings in UCM than in BEM, which could be another reason
424 of the higher nocturnal urban temperature in UCM than in BEM (Figure 14a, c).

425 After increasing the BH in UCM, the building volume increased and absorbed more
426 radiation, in the meanwhile, the SVF decreased and more radiation was trapped in the street
427 canyon. Therefore, the nocturnal urban temperature in UCM increased (Figure 14a, b).

However, the increased BH gave few impacts on urban canopy wind speed in UCM (Figure 15a, b), because the increased BH in UCM was still lower than the 1st model level and did not well interact with lower atmosphere. On the contrary, the urban temperature in BEM decreased after adopting low BH (Figure 14c, d), because total building volume decreased and SVF increased. Meanwhile, as the low BH in BEM reduced the interaction between building and atmosphere, the urban canopy wind speed increased (Figure 15c, d).

When adopting narrow RDW in BEM, the SVF decreased and nocturnal radiation loss reduced. Meanwhile the portion of building area to the total urban area increased, the total building volume increased and absorbed more solar radiation at daytime. Both the above two effect could result in higher urban temperature (Figure 14d, e). When further adopting narrow RFW in BEM, though the total building volume decreased, the number of street canyons increased and the total SVF in the city decreased, urban temperature increased (Figure 14e, f). The narrow RDW and RFW reduced the urban canopy wind speed (Figure 15d, e, f), because they increased urban roughness.

4. Discussion and conclusion

The performance of four urban schemes and two PBL schemes in the WRF model was evaluated over the DFW urban area during a dry summer and a wet summer. All urban schemes overestimated the daytime 2m temperature. BULK gave the largest overestimation of 2m temperature at daytime. At nighttime, only BULK overestimated the 2m temperature, and BEP gave the largest underestimation of 2m temperature.

BULK predicted the strongest daytime UHI during the two summers, while BEP and BEM predicted the weakest daytime UHI (with daytime UCI in dry summer). All urban

schemes produced the nocturnal UHI in the two summers, with overestimation in BULK, underestimation in BEP, and the best performance from UCM and BEM.

BULK and UCM overestimated 10m wind speed, but BEP and BEM underestimated 10m wind speed. Previous studies has attributed the overestimation of 10m wind speed in BULK and UCM to either improper urban description in model (Reames and Stensrud 2017) or unbalances coupling between urban schemes and PBL schemes (Hu et al. 2016). When coupled with MYJ, BULK and UCM produce weaker urban wind speed than rural wind speed at daytime, while when coupled with YSU, UCM produced stronger urban wind speed than rural wind speed at daytime. However, at nighttime, no matter coupled with MYJ or YSU, both BULK and UCM produced erroneous stronger urban wind speed than rural wind speed. This meant that unbalanced coupling between urban schemes and PBL schemes was one reason for the overestimation of wind speed within the city and simulating nocturnal urban canopy wind speed was more challenging for urban schemes and PBL schemes. When using BEP and BEM, the urban wind speed was better reproduced at both daytime and nighttime, which meant using a proper urban scheme with an improved description of urban roughness could significantly improve the simulation of the urban wind field. Thus, we identify that both deficiencies should be responsible for model bias of urban wind speed, and the proper description of urban in model is more critical.

For urban boundary layer simulation, PBL schemes were more dominant than urban schemes, and MYJ was generally superior to YSU. At daytime, MYJ predicted PBLH and wind speed better than YSU did. At nighttime, UCM+MYJ predicted the Θ profiles better than other configurations. In dry summer, MYJ predicted better nocturnal PBL jet strength and nose location than YSU, while in wet summer YSU's performance was improved but

still inferior to MYJ. The shapes of the simulated Θ and QV profiles were close to observation, but the bias of both profiles was large probably because of soil moisture bias in NARR.

The nocturnal PBL stability simulated by the four urban schemes were different because of their different surface cooling rates, with BULK predicting the most unstable PBL and BEP predicting the most stable PBL. The urban schemes had obvious effects on the daytime PBL wind speed profiles because of strong daytime land-atmosphere coupling, while at nighttime urban schemes' impact on PBL wind speed profiles were weak because PBL was decoupled from the surface.

Generally, UCM and BEM showed a better performance than BULK and BEP, though significant difference existed between UCM and BEM. For better understanding the difference between UCM and BEM, we examined model sensitivity to urban geometry parameters. The simulation results showed that urban geometry parameters, BH, RDW and RFW, all play roles in determining urban temperature and wind speed. The three parameters affected urban temperature by determining the SVF and the total building volume in the city and affected urban wind speed by determining the depth and number of the street canyon. In general, the BH has positive correlation with 2m temperature and negative correlation with 10m wind speed; RDW and RFW have negative correlation with 2m temperature and positive correlation with 10m wind speed. The lower BH in UCM should be partially responsible for its overestimation of wind speed, and the larger SVF in BEM should be partially responsible for its underestimation of temperature.

The initial status of land surface, such as soil moisture and soil type, also affect model performance over urban areas. A few efforts have been attempted to improving soil

moisture status, including HRLDAS (Chen et al. 2007) and implementing urban hydrology scheme in UCM (Yang et al. 2014). The HRLDAS is an offline land surface model to spin up the initial land surface property through long offline simulation. The performance of UCM hydrology scheme has been actively evaluated (Yang et al. 2014; Yang et al. 2016; Brownlee et al. 2017).

HRLDAS treats the urban as a concrete surface like the BULK land surface treatment does (Chen et al. 2007). The concrete urban surface in HRLDAS is impervious, thus the urban soil simulated by HRLDAS is usually drier than the surrounding rural soil (Reames and Stensrud 2017; Sharma et al. 2017). In wet summer, urban irrigation effect is negligible compared to abundant rainfall and less rainfall is absorbed by the impervious urban surface than the rural soil, so urban soil becomes drier than rural soil. However, in dry summer, the urban irrigation effect dominates the rainfall effect, therefore urban soil is wetter than the rural soil, which HRLDAS cannot reproduce but UCM with urban irrigation scheme can (Yang et al. 2014; Yang et al. 2016). In summary, when urban soil is drier than rural soil, HRLDAS usually give better performance in wet season/climate with a stronger UHI intensity, due to its crude/inappropriate totally impervious urban treatment.

Improving WRF urban simulation has to be through better understanding of urban processes and better calibration of urban parameters with the improved understanding of urban processes. For the urban schemes, further improvement may be achieved through fixing the unrealistic treatment of momentum in UCM and providing realistic urban parameters in UCM and BEM for more cities.

Acknowledgments. The authors would like to thank the financial support from CAPS, OU and supervising from Drs. Petra Klein and Ming Xue. The first author was partially supported by two grants from the National Key Research and Development Program of China (2018YFB1502803 and 2018YFB0505000). The second author was partially supported by NSF Grant AGS-1917701 and a DOE ASR project.

Reference

Barlage, M., S. G. Miao, and F. Chen, 2016: Impact of physics parameterizations on high-resolution weather prediction over two Chinese megacities. *J Geophys Res-Atmos*, **121,** 4487-4498.

Bougeault, P., and P. Lacarrere, 1989: Parameterization of Orography-Induced Turbulence in a Mesobeta-Scale Model. *Monthly Weather Review*, **117,** 1872-1890.

Brownlee, J., P. Ray, M. Tewari, and H. Tan, 2017: Relative role of turbulent and radiative flux on the near surface temperature in a Single-Layer Urban Canopy Model over Houston. *Journal of Applied Meteorology and Climatology*.

Chen, F., and J. Dudhia, 2001: Coupling an Advanced Land Surface–Hydrology Model with the Penn State–NCAR MM5 Modeling System. Part I: Model Implementation and Sensitivity. *Monthly Weather Review*, **129,** 569-585.

Chen, F., and Coauthors, 2007: Description and Evaluation of the Characteristics of the NCAR High-Resolution Land Data Assimilation System. *Journal of Applied Meteorology and Climatology*, **46,** 694-713.

Ching, J., and Coauthors, 2009: National Urban Database and Access Portal Tool. *Bulletin of the American Meteorological Society*, **90,** 1157-1168.

Christen, A., and R. Vogt, 2004: Energy and radiation balance of a central European city. *International Journal of Climatology*, **24,** 1395-1421.

Dudhia, J., 1989: Numerical Study of Convection Observed during the Winter Monsoon Experiment Using a Mesoscale Two-Dimensional Model. *Journal of the Atmospheric Sciences*, **46,** 3077-3107.

Georgescu, M., P. E. Morefield, B. G. Bierwagen, and C. P. Weaver, 2014: Urban adaptation can roll back warming of emerging megapolitan regions. *P Natl Acad Sci USA*, **111,** 2909-2914.

Grimmond, C. S. B., 1992: The suburban energy balance: Methodological considerations and results for a mid-latitude west coast city under winter and spring conditions. *International Journal of Climatology*, **12,** 481-497.

Gutierrez, E., J. E. Gonzalez, A. Martilli, R. Bornstein, and M. Arend, 2015: Simulations of a Heat-Wave Event in New York City Using a Multilayer Urban Parameterization. *Journal of Applied Meteorology and Climatology*, **54,** 283-301.

Hendricks, E. A., J. C. Knievel, and Y. Wang, 2020: Addition of multilayer urban canopy models to a nonlocal planetary boundary layer parameterization and evaluation using ideal and real cases. *Journal of Applied Meteorology and Climatology*.

Hong, S.-Y., J. Dudhia, and S.-H. Chen, 2004: A Revised Approach to Ice Microphysical Processes for the Bulk Parameterization of Clouds and Precipitation. *Monthly Weather Review*, **132,** 103-120.

Hong, S. Y., Y. Noh, and J. Dudhia, 2006: A new vertical diffusion package with an explicit treatment of entrainment processes. *Monthly Weather Review*, **134,** 2318-2341.

Hu, X.-M., and M. Xue, 2016: Influence of Synoptic Sea-Breeze Fronts on the Urban Heat Island Intensity in Dallas–Fort Worth, Texas. *Monthly Weather Review*, **144,** 1487-1507.

Hu, X.-M., F. Zhang, and J. W. Nielsen-Gammon, 2010a: Ensemble-based simultaneous state and parameter estimation for treatment of mesoscale model error: A real-data study. *Geophysical Research Letters*, **37**.

566 Hu, X. M., J. W. Nielsen-Gammon, and F. Q. Zhang, 2010b: Evaluation of Three Planetary
567 Boundary Layer Schemes in the WRF Model. *Journal of Applied Meteorology and*
568 *Climatology*, **49,** 1831-1844.
569 Hu, X. M., M. Xue, P. M. Klein, B. G. Illston, and S. Chen, 2016: Analysis of Urban Effects in
570 Oklahoma City using a Dense Surface Observing Network. *Journal of Applied*
571 *Meteorology and Climatology*, **55,** 723-741.
572 Jänicke, B., F. Meier, D. Fenner, U. Fehrenbach, A. Holtmann, and D. Scherer, 2017: Urban-rural
573 differences in near-surface air temperature as resolved by the Central Europe Refined
574 analysis (CER): sensitivity to planetary boundary layer schemes and urban canopy models.
575 *International Journal of Climatology*, **37,** 2063-2079.
576 Janjic, Z. I., 1994: The Step-Mountain Eta Coordinate Model - Further Developments of the
577 Convection, Viscous Sublayer, and Turbulence Closure Schemes. *Monthly Weather*
578 *Review*, **122,** 927-945.
579 Janjić, Z. I., 1990: The Step-Mountain Coordinate: Physical Package. *Monthly Weather Review*,
580 **118,** 1429-1443.
581 Kain, J. S., 2004: The Kain–Fritsch Convective Parameterization: An Update. *Journal of Applied*
582 *Meteorology*, **43,** 170-181.
583 Kusaka, H., and F. Kimura, 2004a: Coupling a single-layer urban canopy model with a simple
584 atmospheric model: Impact on urban heat island simulation for an idealized case. *J*
585 *Meteorol Soc Jpn*, **82,** 67-80.
586 ——, 2004b: Thermal effects of urban canyon structure on the nocturnal heat island: Numerical
587 experiment using a mesoscale model coupled with an urban canopy model. *Journal of*
588 *Applied Meteorology*, **43,** 1899-1910.
589 Kusaka, H., H. Kondo, Y. Kikegawa, and F. Kimura, 2001: A simple single-layer urban canopy
590 model for atmospheric models: Comparison with multi-layer and slab models. *Boundary-*
591 *Layer Meteorology*, **101,** 329-358.

592 Lee, S. H., S. A. McKeen, and D. J. Sailor, 2014: A regression approach for estimation of
593 anthropogenic heat flux based on a bottom-up air pollutant emission database. *Atmospheric*
594 *Environment*, **95,** 629-633.
595 Li, D., E. Bou-Zeid, M. Barlage, F. Chen, and J. A. Smith, 2013: Development and evaluation of a
596 mosaic approach in the WRF-Noah framework. *Journal of Geophysical Research:*
597 *Atmospheres*, **118,** 11,918-911,935.
598 Liao, J. B., T. J. Wang, X. M. Wang, M. Xie, Z. Q. Jiang, X. X. Huang, and J. L. Zhu, 2014: Impacts
599 of different urban canopy schemes in WRF/Chem on regional climate and air quality in
600 Yangtze River Delta, China. *Atmospheric Research*, **145,** 226-243.
601 Liu, Y., F. Chen, T. Warner, and J. Basara, 2006: Verification of a Mesoscale Data-Assimilation
602 and Forecasting System for the Oklahoma City Area during the Joint Urban 2003 Field
603 Project. *Journal of Applied Meteorology and Climatology*, **45,** 912-929.
604 Martilli, A., 2002: Numerical study of urban impact on boundary layer structure: Sensitivity to
605 wind speed, urban morphology, and rural soil moisture. *Journal of Applied Meteorology*,
606 **41,** 1247-1266.
607 Martilli, A., A. Clappier, and M. W. Rotach, 2002: An urban surface exchange parameterisation
608 for mesoscale models. *Boundary-Layer Meteorology*, **104,** 261-304.
609 Mlawer, E. J., S. J. Taubman, P. D. Brown, M. J. Iacono, and S. A. Clough, 1997: Radiative transfer
610 for inhomogeneous atmospheres: RRTM, a validated correlated-k model for the longwave.
611 *Journal of Geophysical Research: Atmospheres*, **102,** 16663-16682.
612 Nemunaitis-Berry, K. L., P. M. Klein, J. B. Basara, and E. Fedorovich, 2017: Sensitivity of
613 Predictions of the Urban Surface Energy Balance and Heat Island to Variations of Urban
614 Canopy Parameters in Simulations with the WRF Model. *Journal of Applied Meteorology*
615 *and Climatology*, **56,** 573-595.
616 Oke, T. R., 1982: The Energetic Basis of the Urban Heat-Island. *Quarterly Journal of the Royal*
617 *Meteorological Society*, **108,** 1-24.

618 ——, 1988: The Urban Energy Balance. *Prog Phys Geog*, **12,** 471-508.
619 Reames, L. J., and D. J. Stensrud, 2017: Sensitivity of Simulated Urban–Atmosphere Interactions
620 in Oklahoma City to Urban Parameterization. *Journal of Applied Meteorology and*
621 *Climatology*, **56,** 1405-1430.
622 Sailor, D. J., M. Georgescu, J. M. Milne, and M. A. Hart, 2015: Development of a national
623 anthropogenic heating database with an extrapolation for international cities. *Atmospheric*
624 *Environment*, **118,** 7-18.
625 Salamanca, F., and A. Martilli, 2009: A new Building Energy Model coupled with an Urban
626 Canopy Parameterization for urban climate simulations—part II. Validation with one
627 dimension off-line simulations. *Theoretical and Applied Climatology*, **99,** 345-356.
628 Salamanca, F., A. Krpo, A. Martilli, and A. Clappier, 2009: A new building energy model coupled
629 with an urban canopy parameterization for urban climate simulations—part I. formulation,
630 verification, and sensitivity analysis of the model. *Theoretical and Applied Climatology*,
631 **99,** 331-344.
632 Salamanca, F., A. Martilli, M. Tewari, and F. Chen, 2011: A Study of the Urban Boundary Layer
633 Using Different Urban Parameterizations and High-Resolution Urban Canopy Parameters
634 with WRF. *Journal of Applied Meteorology and Climatology*, **50,** 1107-1128.
635 Salamanca, F., M. Georgescu, A. Mahalov, and M. Moustaoui, 2015: Summertime Response of
636 Temperature and Cooling Energy Demand to Urban Expansion in a Semiarid Environment.
637 *Journal of Applied Meteorology and Climatology*, **54,** 1756-1772.
638 Sharma, A., H. J. S. Fernando, A. F. Hamlet, J. J. Hellmann, M. Barlage, and F. Chen, 2017: Urban
639 meteorological modeling using WRF: a sensitivity study. *International Journal of*
640 *Climatology*, **37,** 1885-1900.
641 Stewart, I. D., and T. R. Oke, 2012: Local Climate Zones for Urban Temperature Studies. *Bulletin*
642 *of the American Meteorological Society*, **93,** 1879-1900.

643 Taha, H., 1999: Modifying a Mesoscale Meteorological Model to Better Incorporate Urban Heat
644 Storage: A Bulk-Parameterization Approach. *Journal of Applied Meteorology*, **38,** 466-
645 473.
646 United Nations Department of Economic and Social Affairs, P. D., 2012: United Nations
647 Department of Economic and Social Affairs, Population Division, 2012: World
648 urbanization prospects, the 2011 revision.
649 Wickham, J., C. A. Barnes, M. S. Nash, and T. G. Wade, 2015: Combining NLCD and MODIS to
650 create a land cover-albedo database for the continental United States. *Remote Sensing of*
651 *Environment*, **170,** 143-152.
652 Winguth, A. M. E., and B. Kelp, 2013: The Urban Heat Island of the North-Central Texas Region
653 and Its Relation to the 2011 Severe Texas Drought. *Journal of Applied Meteorology and*
654 *Climatology*, **52,** 2418-2433.
655 Yang, J., Z.-H. Wang, M. Georgescu, F. Chen, and M. Tewari, 2016: Assessing the Impact of
656 Enhanced Hydrological Processes on Urban Hydrometeorology with Application to Two
657 Cities in Contrasting Climates. *Journal of Hydrometeorology*, **17,** 1031-1047.
658 Yang, J., Z.-H. Wang, F. Chen, S. Miao, M. Tewari, J. A. Voogt, and S. Myint, 2014: Enhancing
659 Hydrologic Modelling in the Coupled Weather Research and Forecasting–Urban
660 Modelling System. *Boundary-Layer Meteorology*, **155,** 87-109.
661
662
663
664
665
666

Tables

Figures Captions

Figure 1. (a) Configuration of the 4 two-way nested domains for simulation. Shading is terrain height in meters. (b) NLCD 40 classes land-cover maps for D4. (c) Updated representative diurnal profiles of AH.

Figure 2. TCEQ stations in (a) July 2011 and (b) July 2015 overlaid on imperviousness (unit, %) from NLCD 2011. The blue background is water body. The blue star denotes the location of the Fort Worth radiosonde. The 5 red diamonds denote the locations of the selected urban stations, and the 8 blue squares denote the locations of the selected rural stations.

Figure 3. Same to Figure 2 but for the spatial distribution of early evening transition cooling rate of TCEQ stations in (c) July 2011 and (d) July 2015.

Figure 4. Observed and simulated mean diurnal variation of (a,b) 2m temperature, (c,d) 10m wind speed (e,f) 2m relative humidity, (g,h) 2m dewpoint at 5 urban stations during (left) July 2011, and (right) July 2015. The 5 urban stations are denoted by red diamonds in Figure 2.

Figure 5. Simulated mean diurnal variation of (a,b) net radiation, (c,d) sensible heat flux, (e,f) latent heat flux, (g,h) ground heat flux at 5 urban stations during (left) July 2011 and (right) July 2015.

Figure 6. Observed mean UHI intensity (colored dots) with respect to the average of the 8 rural stations at (a,b) daytime (0800CST~1700CST) and (c,d) nighttime (2000CST~0500CST) in (left) July 2011 and (right) July 2015. The gray-black background is imperviousness (%) from NLCD 2011 and the blue background is water body.

Figure 7. Same to Figure 6, but for wind speed (colored dots) and wind vector (black arrow). The horizontal arrow on the left-bottom of figures denotes the reference vector ($5\mathrm{m\ s-1}$).

Figure 8. Daytime averaged (0800CST~1700CST) 2m UHI in (top) July 2011 and (bottom) July 2015 simulated by (a,f) BULK+MYJ, (b,g) UCM+MYJ, (c,h) UCM+YSU, (d,i)

712 BEP+MYJ, (e,j) BEM+MYJ. The UHI was calculated by the 2m temperature minus the
713 average of the 8 rural stations.
714 Figure 9. Same to Figure 8 but for 10m wind speed.
715 Figure 10. Vertical profiles of (a,b) potential temperature, (c,d) wind speed, (e,f) water vapor at
716 1700CST in (left) July 2011, and (right) July 2015 observed from SPARC sounding (black
717 line) and simulated with BULK+MYJ (red lines), UCM+MYJ (orange lines), UCM+YSU
718 (green lines), BEP+MYJ (blue lines) and BEM+MYJ (purple lines).
719 Figure 11. Same to Figure 8 but for nocturnal average (2000CST~0500CST).
720 Figure 12. Same to Figure 9 but for nocturnal average (2000CST~0500CST).
721 Figure 13. Same to Figure 10, but at 0500CST.
722 Figure 14. The nocturnal averaged (2000CST~0500CST) 2m temperature simulated with different
723 urban geometry parameters.
724 Figure 15. Same to Figure 14, but for 10m wind speed.
725
726

Tables

Index	NLCD Description	Percentage
17	Open Water (OW)	4.5756% Rural
22	Perennial Ice/Snow (PIS)	0% Rural
23	Developed, Open Space (DOS)	41.089771% Urban
24	Developed, Low Intensity (DLI)	30.173161% Urban
25	Developed, Medium Intensity (DMI)	19.59128% Urban
26	Developed, High Intensity (DHI)	9.145788% Urban
27	Barren Land (BL)	0.394785% Rural
28	Deciduous Forest (DF)	16.000927% Rural
29	Evergreen Forest (EF)	2.277274% Rural
30	Mixed Forest (MF)	0.306798% Rural
31	Dwarf Scrub (DS)*	0% Rural
32	Shrub/Scrub (SS)	1.281535% Rural
33	Grassland/Herbaceous (GH)	45.751343% Rural
34	Sedge/Herbaceous (SH)*	0% Rural
35	Lichens (LIC)*	0% Rural
36	Moss (MOS)*	0% Rural
37	Pasture/Hay (PH)	17.329805% Rural
38	Cultivated Crops (CC)	10.498663% Rural
39	Woody Wetlands (WW)	1.316639% Rural
40	Emergent Herbaceous Wetlands (EHW)	0.266632% Rural

Table 1. Description of land-use categories and their corresponding percentages in D4.

Station Name	ST#	STN	LULC	IMP(%)	HGT(m)	Temp	Wind	TD	RH
Greenville	1	GV	17	0.00	162.93	√	√		
Arlington Municipal Airport	2	AMA	25	27.33	176.79	√	√		
Grapevine Fairway	3	GF	33	6.65	174.45	√	√	√	√
Keller	4	KL	33	15.81	222.96	√	√		
Fort Worth Northwest	5	FWN	24	51.53	204.99	√	√	√	√
Eagle Mountain Lake	6	EML	33	0.48	240.10	√	√		
Rockwall Heath	7	RH	25	18.79	159.17	√	√		
Parker County	8	PC	33	0.00	351.18	√	√		
Kaufman	9	KF	24	29.60	133.39	√	√	√	√
Cleburne Airport	10	CBA	23	15.38	258.95	√	√		
Granbury	11	GB	33	4.88	230.14	√	√		
Midlothian OFW	12	MOFW	38	0.07	188.86	√	√		
Denton Airport South	13	DAS	33	2.33	207.66	√	√	√	√
Dallas Redbird Airport Executive	14	DRAE	24	28.55	196.16	√	√		
Dallas North #2	15	DN2	23	32.99	183.75	√	√		
Dallas Hinton	16	DH	25	57.32	143.20	√	√	√	√
Convention Center	17	CC	26	87.09	147.91	√	√		
Frisco Eubanks	18	FE	24	27.65	215.16	√	√		
Frisco	19	FS	25	46.50	230.94	√	√		
Pilot Point	20	PP	33	1.11	207.98	√	√		
Italy	21	IL	28	1.09	161.24	√	√	√	√
Corsicana Airport	22	CSA	33	5.08	132.61	√	√	√	√
Decatur Thompson	23	DT	33	4.92	325.34	√	√		
Flower Mound Shiloh	24	FMS	28	2.20	202.00	√	√		
Johnson County Luisa	25	JCL	23	7.55	208.40	√	√		
Everman Johnson Park	26	EJP	33	21.25	198.85	√	√		

735 Table 2. Information of the TCEQ stations in the DFW metropolitan area in 2011, including
736 their full names, station number, short names, land-use categories, urban fraction/surface
737 imperviousness, elevation, availability of records of temperature, wind, dewpoint, relative
738 humidity.

739

740

741

742

743

Model Level (No.)	Level Height (m)	Model Level (No.)	Level Height (m)	Model Level (No.)	Level Height (m)
1	12	10	369	19	1401
2	36	11	454	20	1633
3	60	12	538	21	1870
4	84	13	624	22	2112
5	109	14	710	23	2385
6	141	15	819	24	2689
7	182	16	951	25	3002
8	224	17	1084	26	3324
9	286	18	1219	27	3657

744 Table 3. The heights of the lowest 27 model level.

745

746

747

748

749

750

751

752

753

754

755

756

757

	low intensity residential	*high intensity residential*	*industrial/commercial*
BH	5.0 m	7.5 m	10.0 m
RDW	8.3 m	9.4 m	10.0 m
RFW	8.3 m	9.4 m	10.0 m

Table 4. Urban geometry parameters (building height, road width, and roof width) used for three urban categories, i.e., low intensity residential area, high intensity residential area, and industrial/commercial area.

	low intensity residential	*high intensity residential*	*industrial/commercial*
BH	5 m – 15 % 10 m – 70 % 15 m – 15 % mean *building height* 10 m	5 m – 0 % 10 m – 20 % 15 m – 60 % 20 m – 20 % mean *building height* 15 m	5 m – 0 % 10 m – 0 % 15 m – 10 % 20 m – 25 % 25 m – 40 % 30 m – 25 % 35 m – 0 % mean *building height* 24 m
RDW	30 m	25 m	20 m
RFW	13 m	17 m	20 m

775 Table 5. Same to Table 4, but used in BEM. The building height in BEM is not fixed as in

776 UCM but classified with different percentages.

777

778

779

780

781

782

783

Experiment Name	*low intensity residential*		*high intensity residential*		*industrial/commercial*	
UCM-CTRL	BH	5.0 m	BH	7.5 m	BH	10.0 m
	RDW	8.3 m	RDW	9.4 m	RDW	10.0 m
	RFW	8.3 m	RFW	9.4 m	RFW	10.0 m
UCM-HBH	BH	8.0 m	BH	10.0 m	BH	12.0 m
	RDW	8.3 m	RDW	9.4 m	RDW	10.0 m
	RFW	8.3 m	RFW	9.4 m	RFW	10.0 m
BEM-CTRL	BH	10.0 m	BH	15.0 m	BH	24.0 m
	RDW	30.0 m	RDW	25.0 m	RDW	20.0 m
	RFW	13.0 m	RFW	17.0 m	RFW	20.0 m
BEM-LBH	BH	5.0 m	BH	7.5 m	BH	10.0 m
	RDW	30.0 m	RDW	25.0 m	RDW	20.0 m
	RFW	13.0 m	RFW	17.0 m	RFW	20.0 m
BEM-LBH-NRDW	BH	5.0 m	BH	7.5 m	BH	10.0 m
	RDW	8.3 m	RDW	9.4 m	RDW	10.0 m
	RFW	13.0 m	RFW	17.0 m	RFW	20.0 m
BEM-LBH-NRDW-NRFW	BH	5.0 m	BH	7.5 m	BH	10.0 m
	RDW	8.3 m	RDW	9.4 m	RDW	10.0 m
	RFW	8.3 m	RFW	9.4 m	RFW	10.0 m

Table 6. The urban geometry parameters in the sensitivity simulations.

Figures

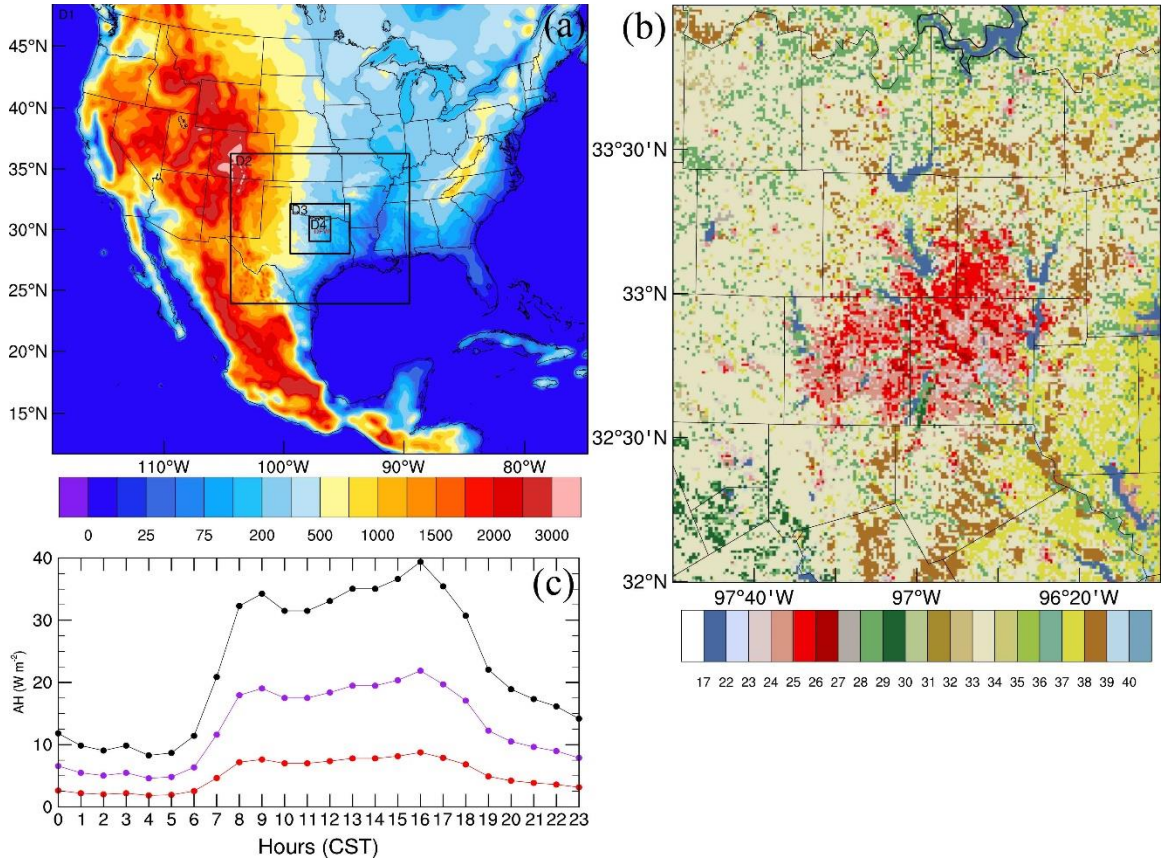

Figure 1. (a) Configuration of the 4 two-way nested domains for simulation. Shading is terrain height in meters. (b) NLCD 40 classes land-cover maps for D4. (c) Updated representative diurnal profiles of AH.

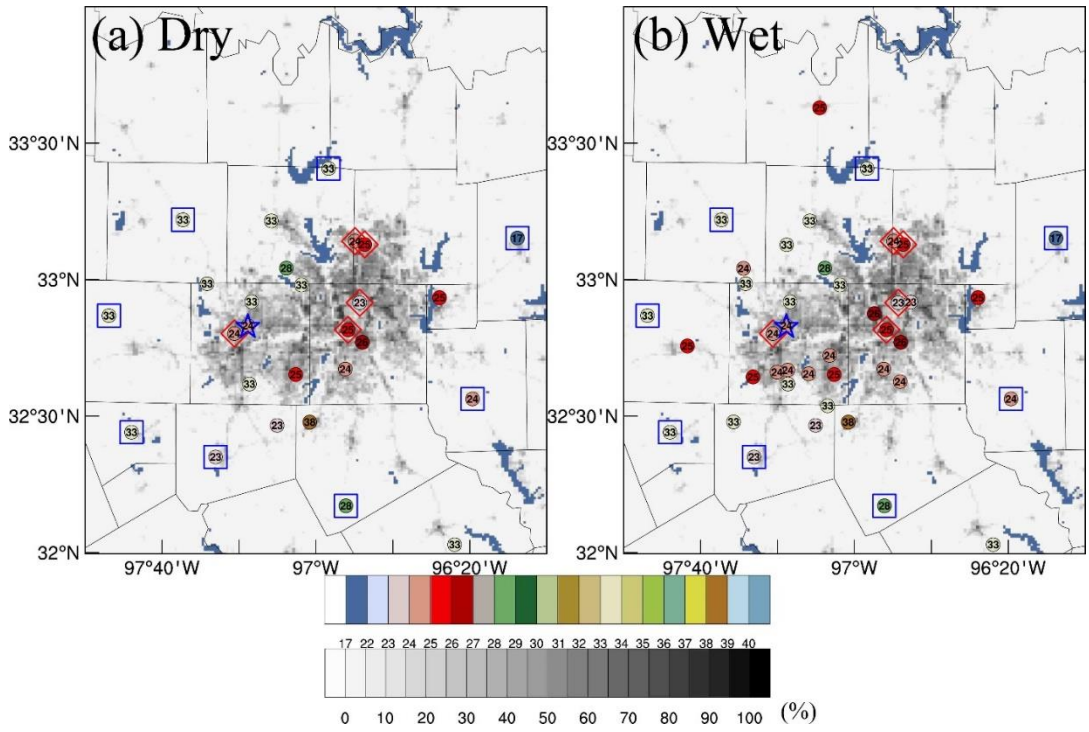

Figure 2. TCEQ stations in (a) July 2011 and (b) July 2015 overlaid on imperviousness (unit, %) from NLCD 2011. The blue background is water body. The blue star denotes the location of the Fort Worth radiosonde. The 5 red diamonds denote the locations of the selected urban stations, and the 8 blue squares denote the locations of the selected rural stations.

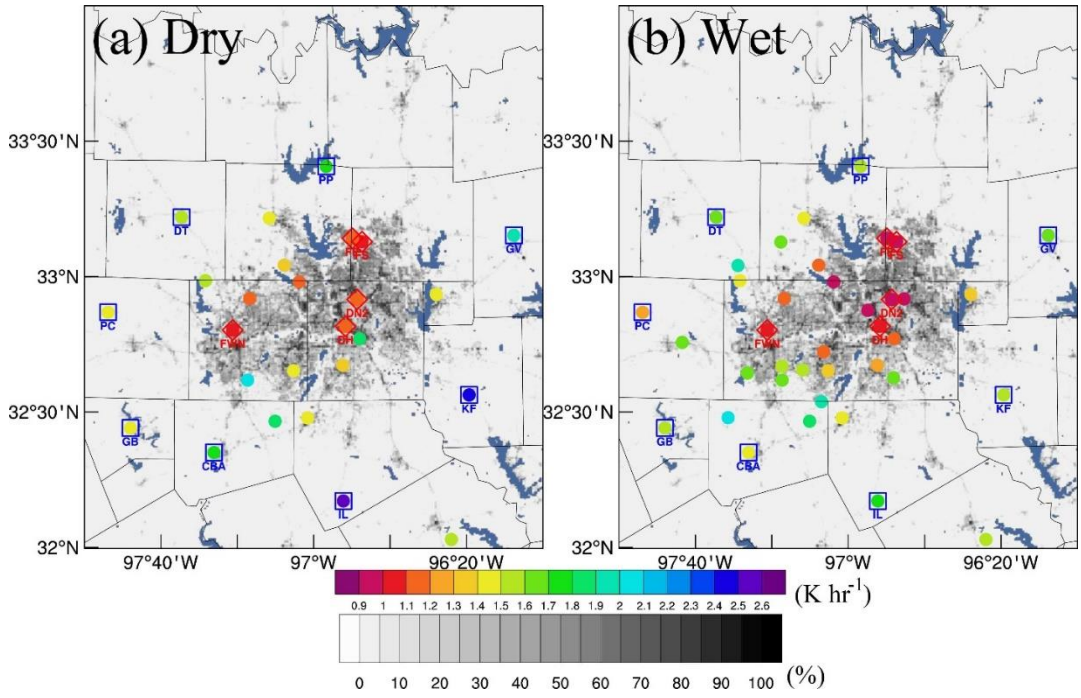

Figure 3. Same to Figure 2 but for the spatial distribution of early evening transition cooling rate of TCEQ stations in (c) July 2011 and (d) July 2015.

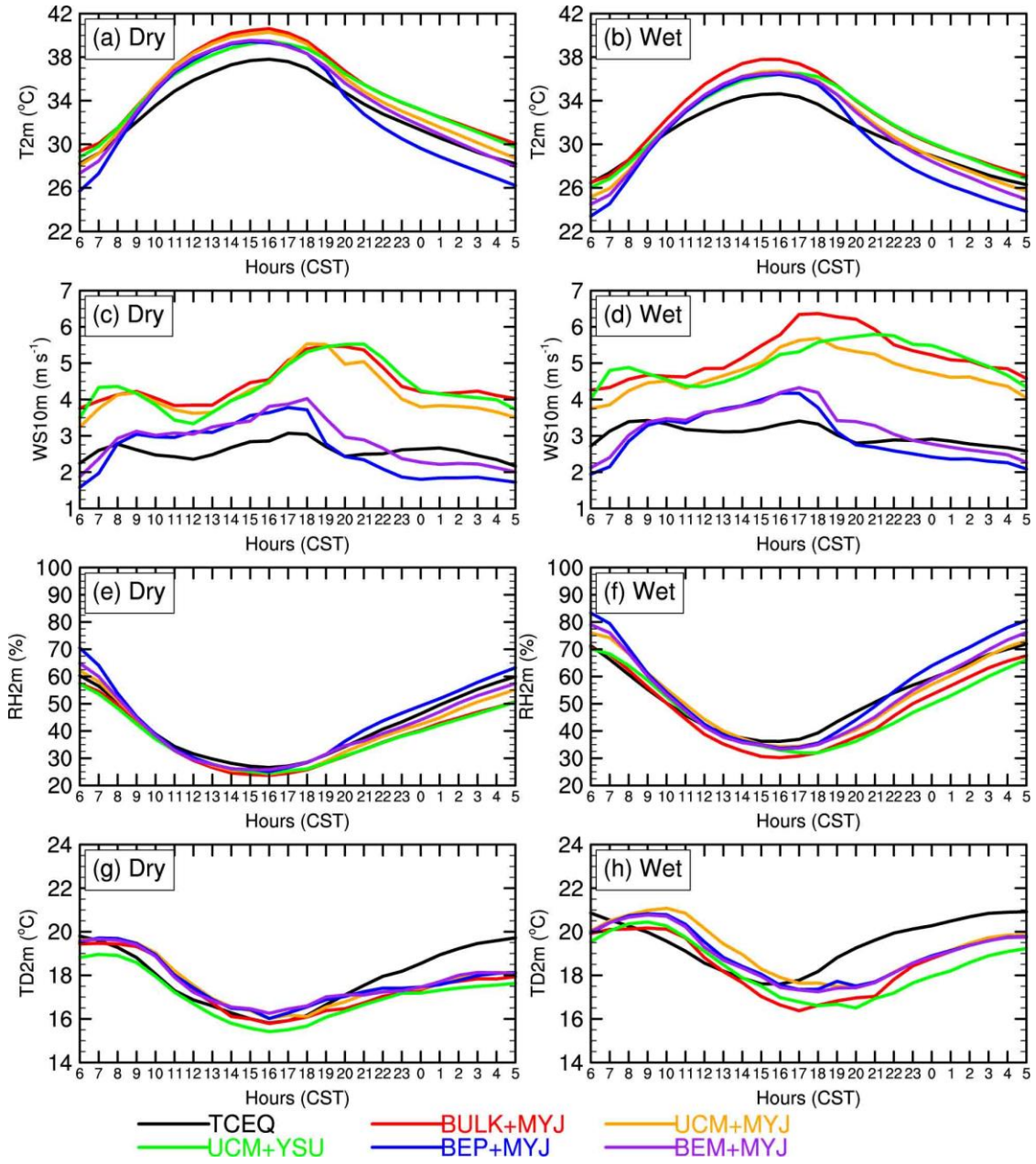

Figure 4. Observed and simulated mean diurnal variation of (a,b) 2m temperature, (c,d) 10m wind speed (e,f) 2m relative humidity, (g,h) 2m dewpoint at 5 urban stations during (left) July 2011, and (right) July 2015. The 5 urban stations are denoted by red diamonds in *Figure 2*.

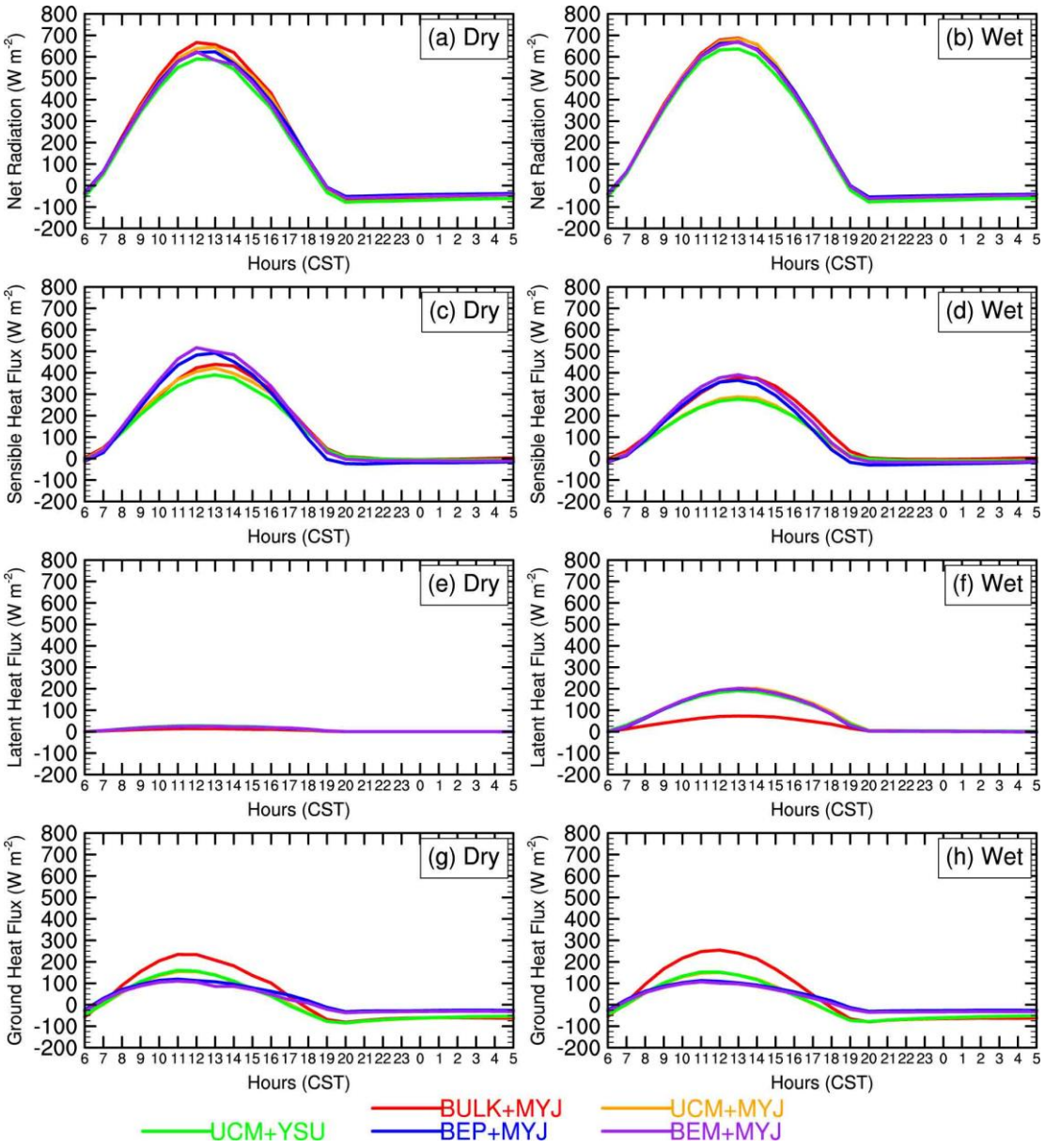

Figure 5. Simulated mean diurnal variation of (a,b) net radiation, (c,d) sensible heat flux, (e,f) latent heat flux, (g,h) ground heat flux at 5 urban stations during (left) July 2011 and (right) July 2015.

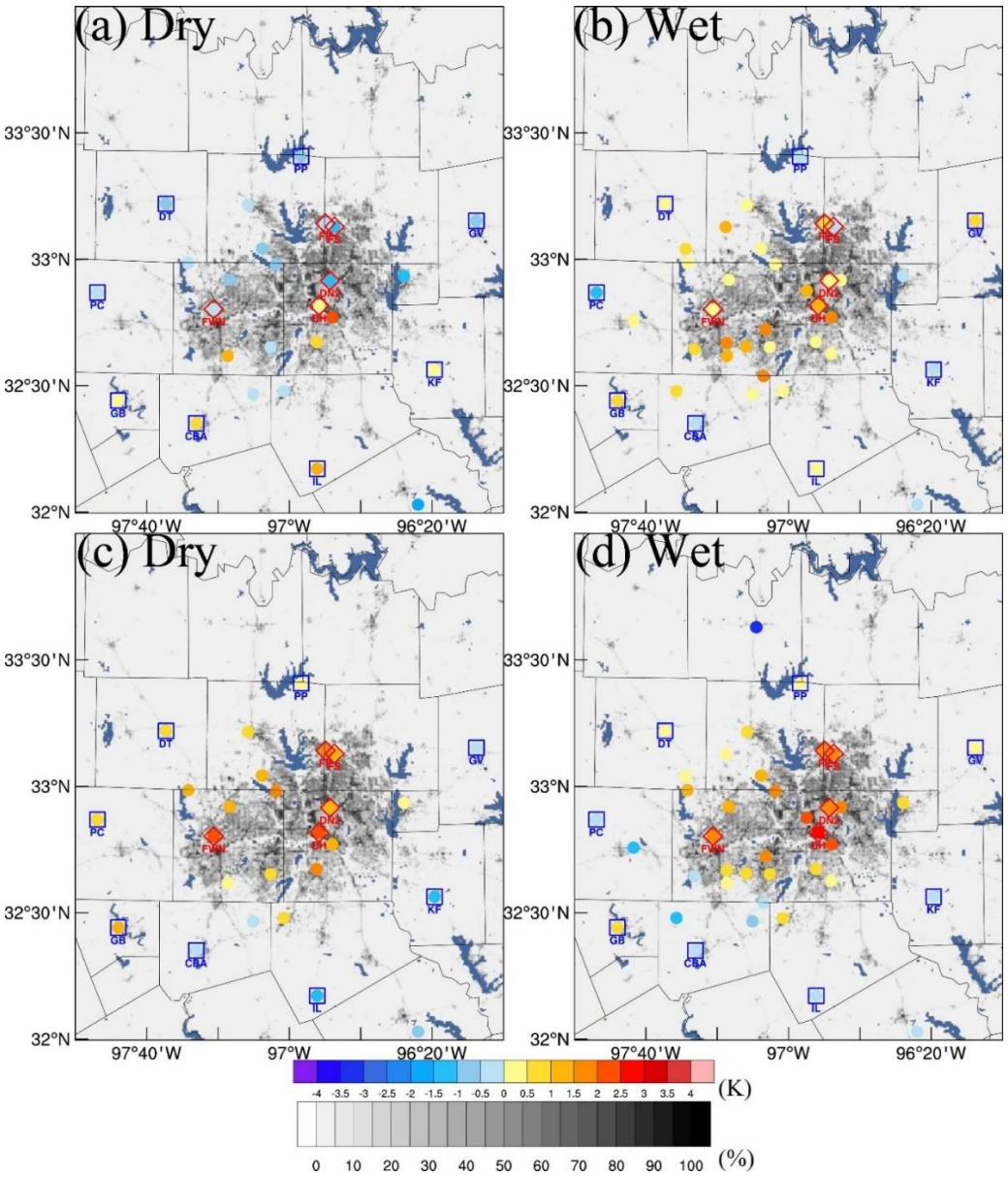

817

818 Figure 6. Observed mean UHI intensity (colored dots) with respect to the average of the 8
819 rural stations at (a,b) daytime (0800CST~1700CST) and (c,d) nighttime
820 (2000CST~0500CST) in (left) July 2011 and (right) July 2015. The gray-black background
821 is imperviousness (%) from NLCD 2011 and the blue background is water body.

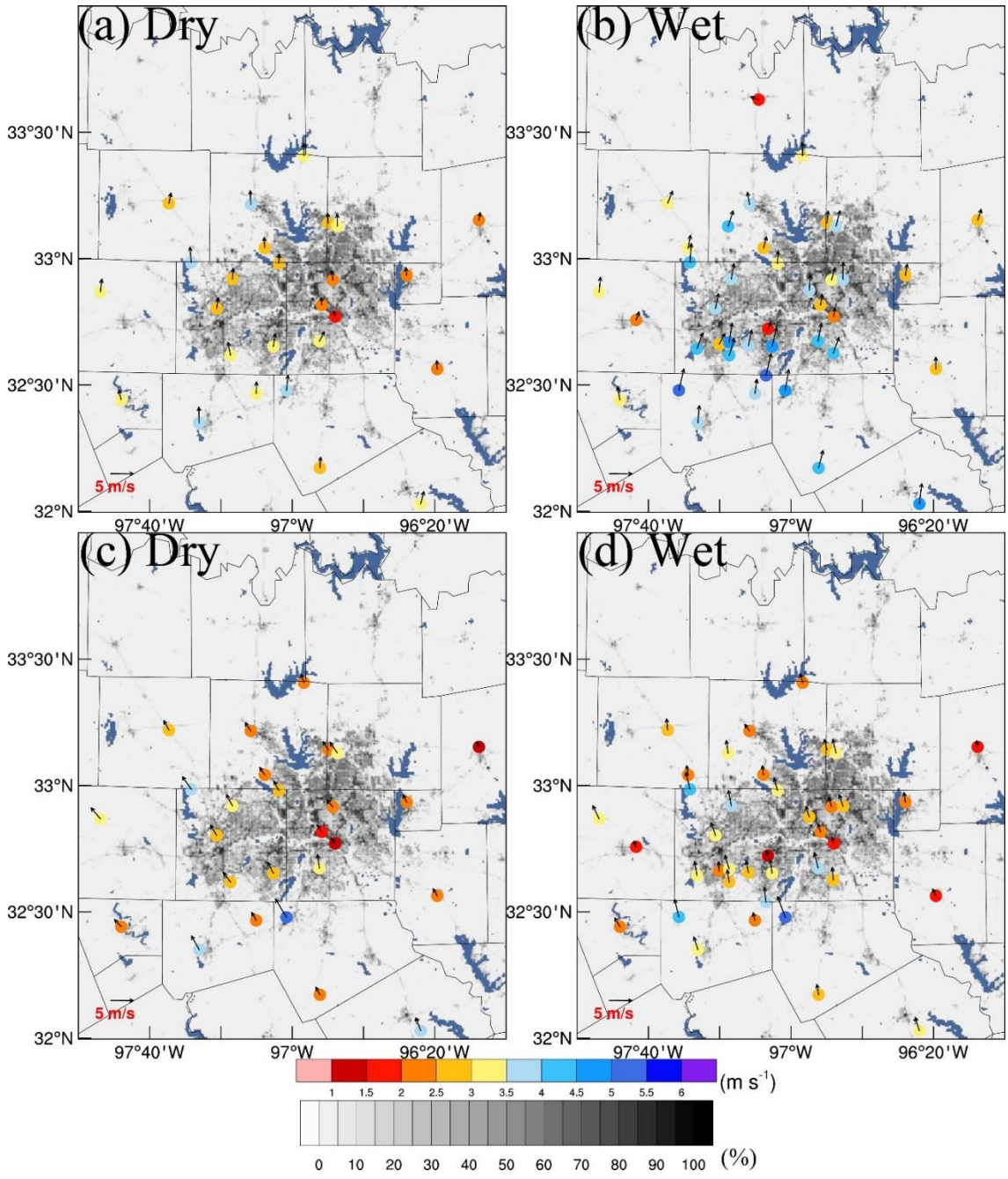

822

823 Figure 7. Same to Figure 6, but for wind speed (colored dots) and wind vector (black arrow).

824 The horizontal arrow on the left-bottom of figures denotes the reference vector ($5m\ s^{-1}$).

825

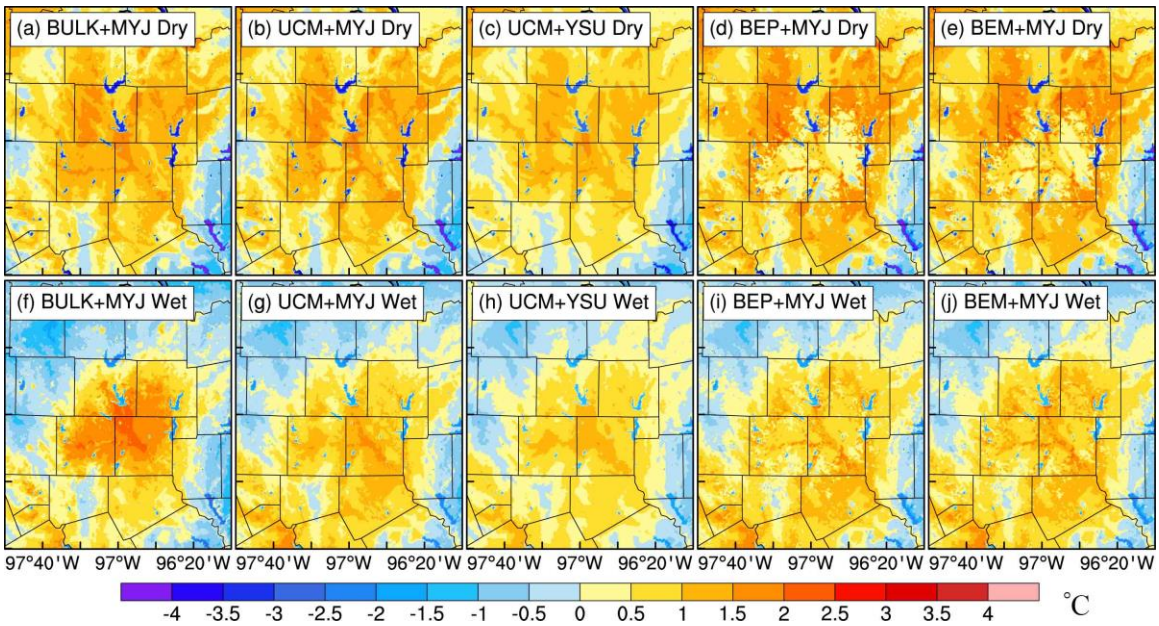

826

827 Figure 8. Daytime averaged (0800CST~1700CST) 2m UHI in (top) July 2011 and (bottom)
828 July 2015 simulated by (a,f) BULK+MYJ, (b,g) UCM+MYJ, (c,h) UCM+YSU, (d,i)
829 BEP+MYJ, (e,j) BEM+MYJ. The UHI was calculated by the 2m temperature minus the
830 average of the 8 rural stations.

831

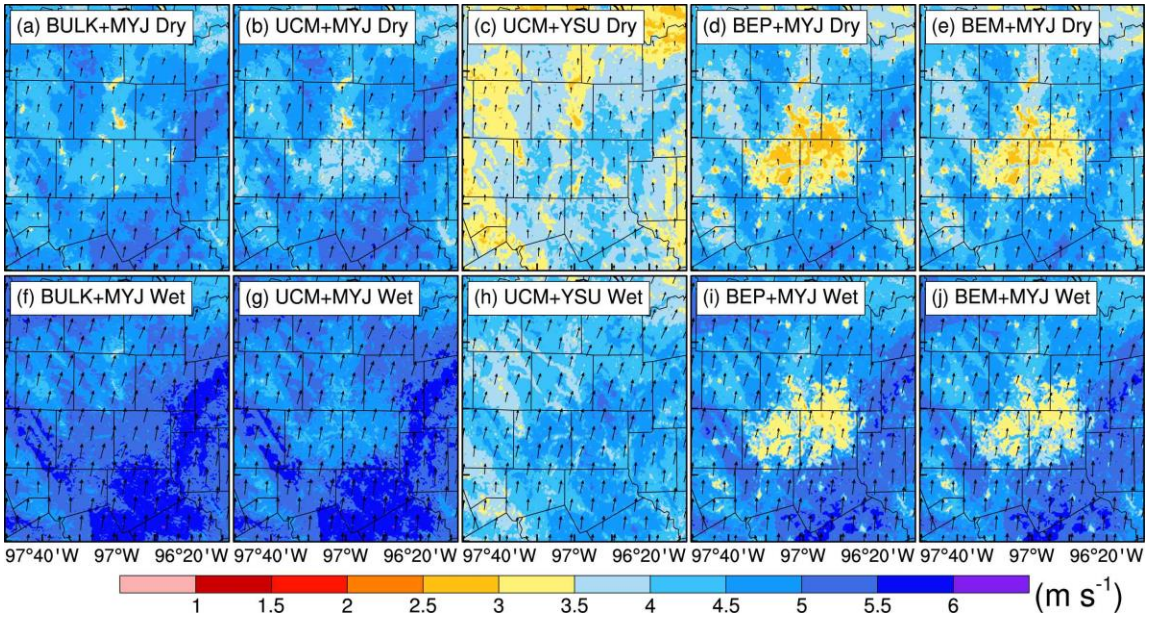

832

833 Figure 9. Same to Figure 8 but for 10m wind speed.

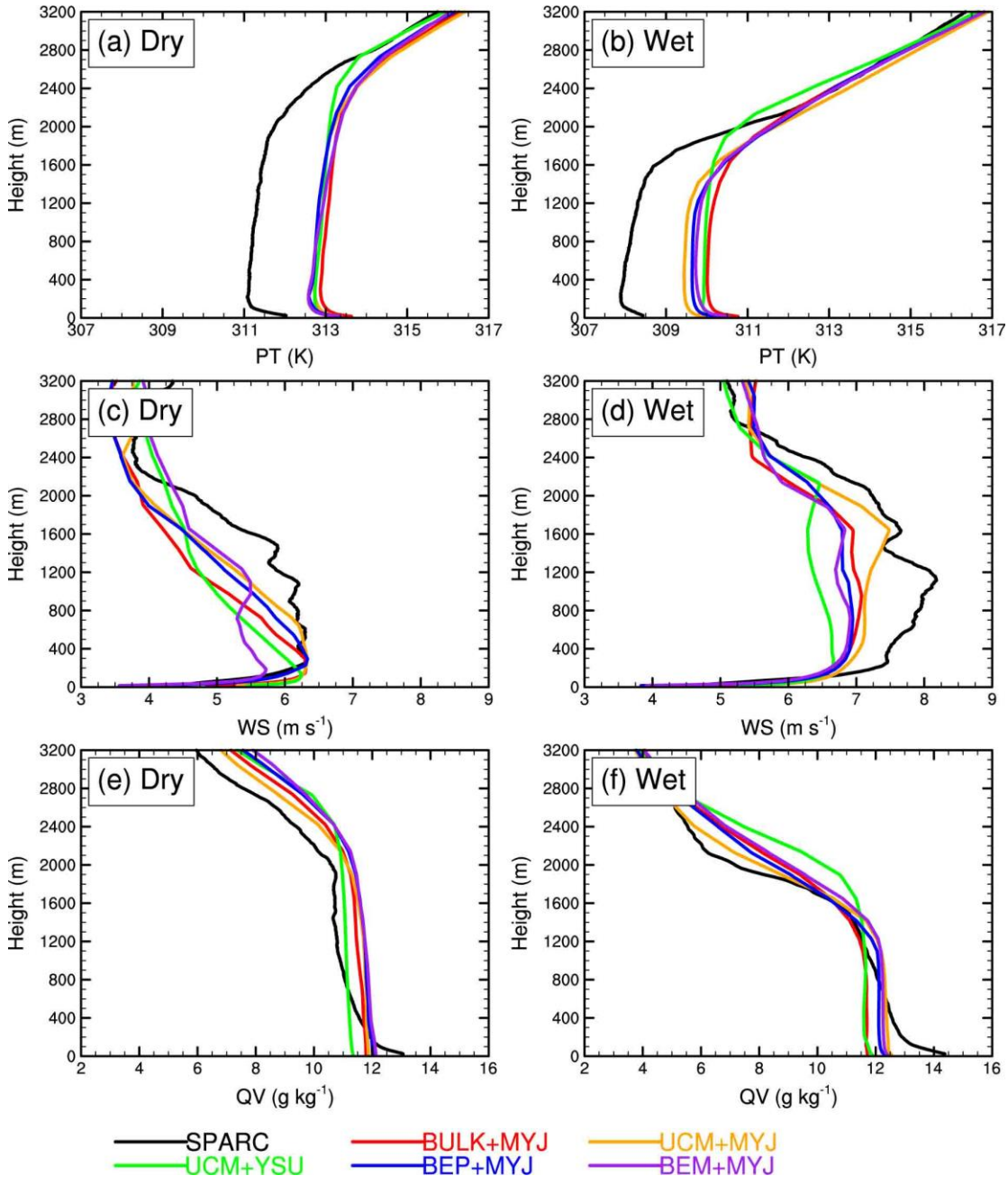

Figure 10. Vertical profiles of (a,b) potential temperature, (c,d) wind speed, (e,f) water vapor at 1700CST in (left) July 2011, and (right) July 2015 observed from SPARC sounding (black line) and simulated with BULK+MYJ (red lines), UCM+MYJ (orange lines), UCM+YSU (green lines), BEP+MYJ (blue lines) and BEM+MYJ (purple lines).

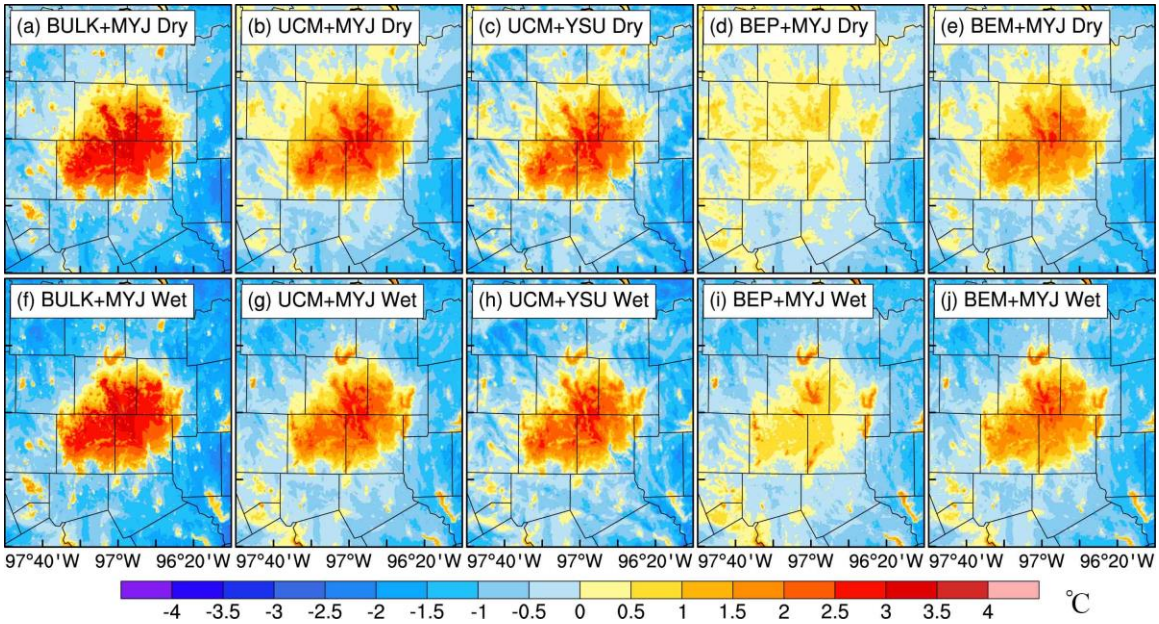

839

840 Figure 11. Same to Figure 8 but for nocturnal average (2000CST~0500CST).

841

842

843

844

845

846

847

848

849

850

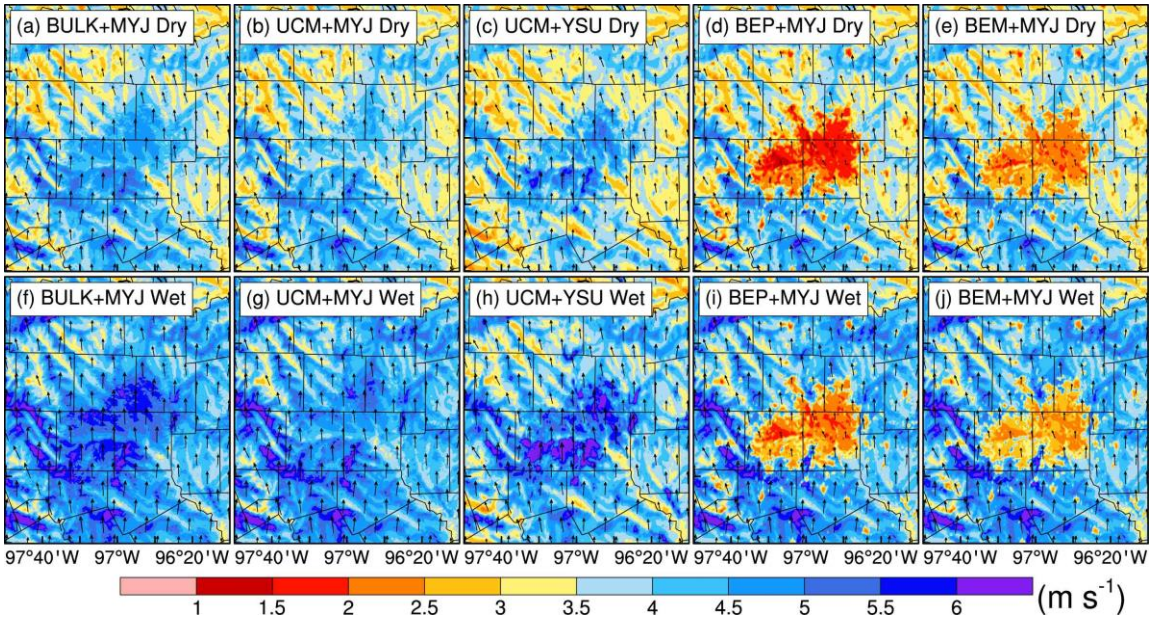

851

852 Figure 12. Same to Figure 9 but for nocturnal average (2000CST~0500CST).

853

854

855

856

857

858

859

860

861

862

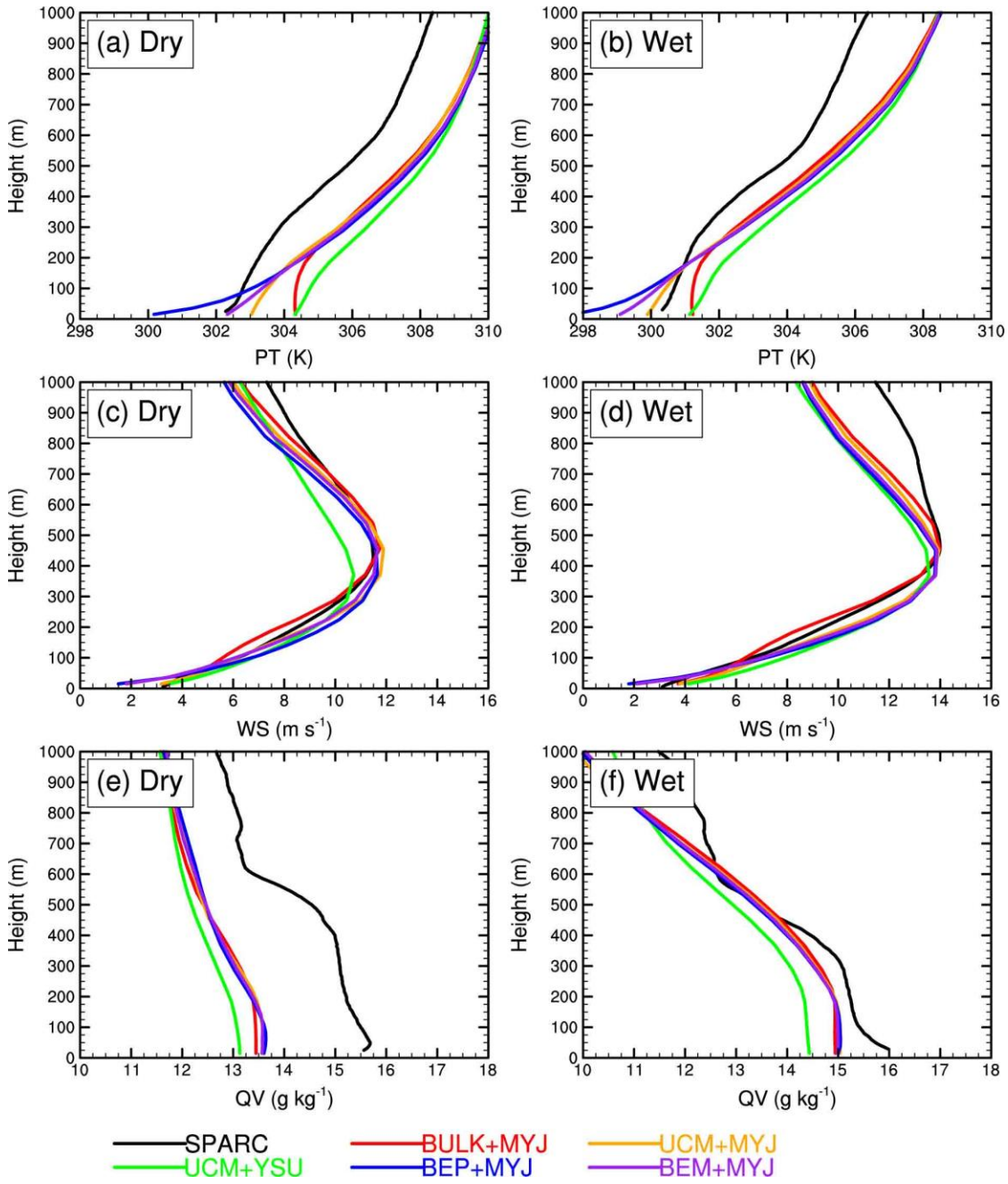

863

864 Figure 13. Same to Figure 10, but at 0500CST.

865

866

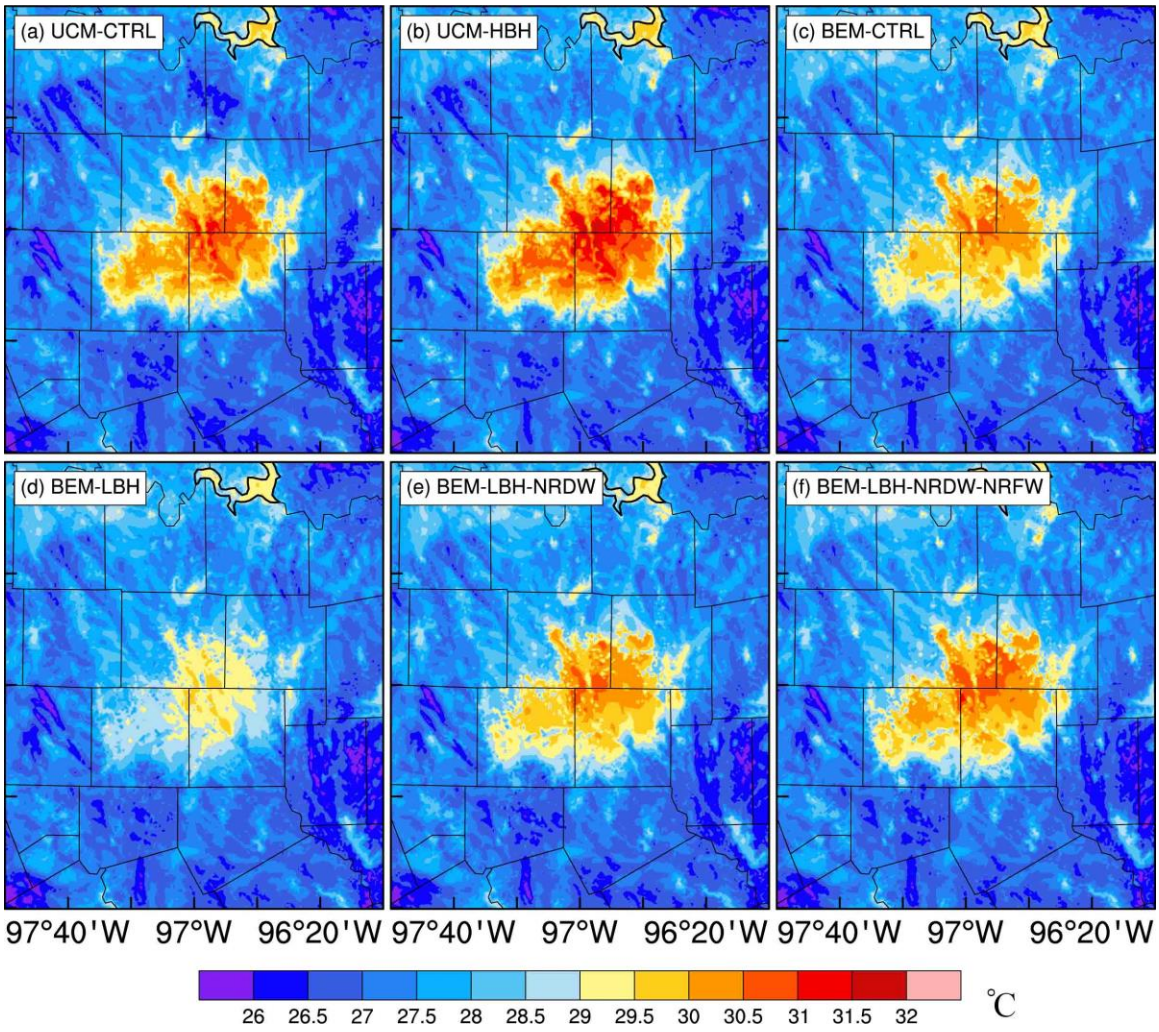

867

868 Figure 14. The nocturnal averaged (2000CST~0500CST) 2m temperature simulated with

869 different urban geometry parameters.

870

871

872

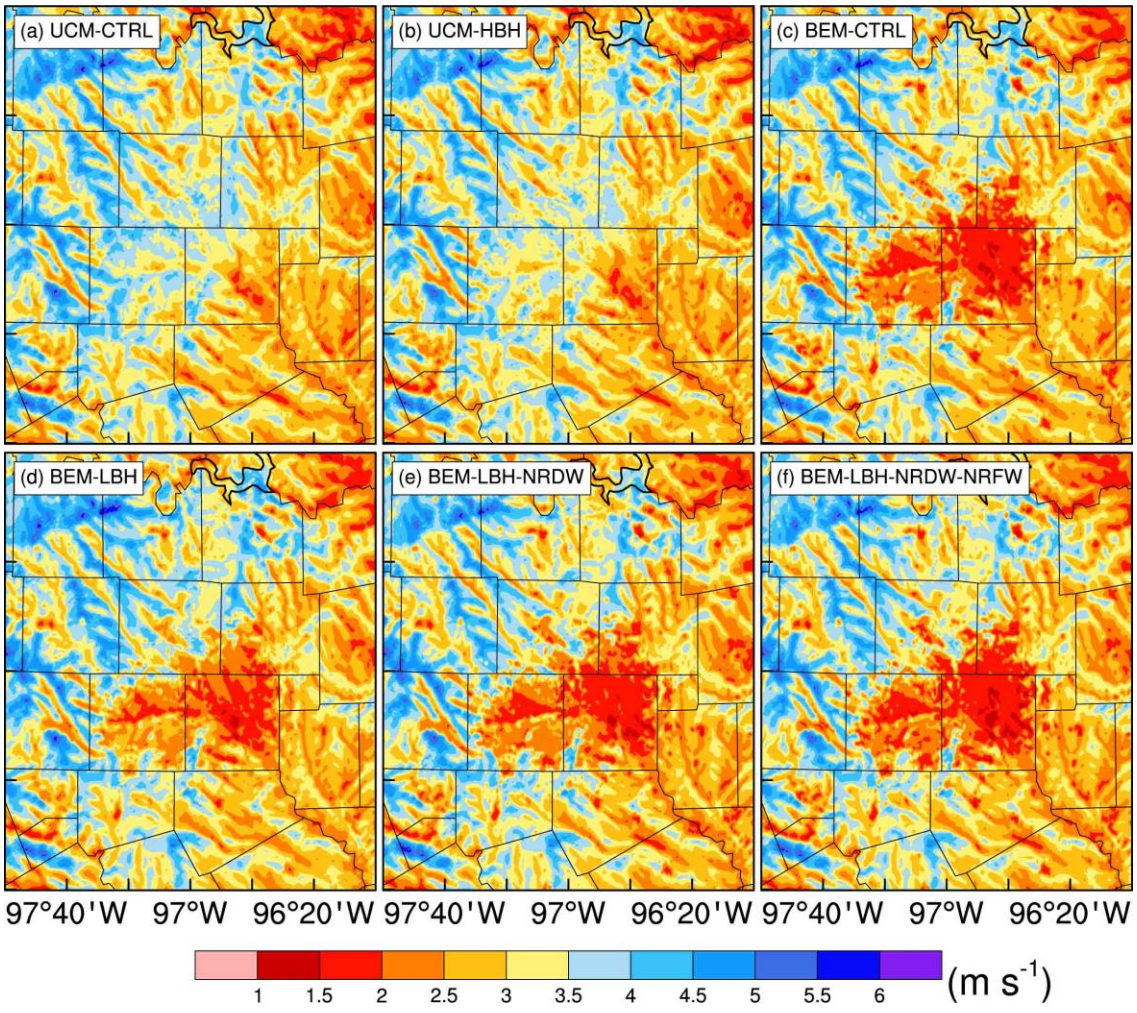

873

874 Figure 15. Same to Figure 14, but for 10m wind speed.

875